ACS APPLIED POLYMER MATERIALS

pubs.acs.org/acsapm Article

Hybrid Microgel–MOF (M&M) Etalon Sensors for In Situ Detection of Dissolved CO_2

Georgia Kontaxi, Klaartje Roovers, Michael J. Serpe, and Hanieh Bazyar*

Cite This: ACS Appl. Polym. Mater. 2026, 8, 1242–1257 Read Online

ACCESS | Metrics & More | Article Recommendations | Supporting Information

ABSTRACT: The continuous rise of atmospheric CO_2 and its associated impacts, including ocean acidification, demand innovative strategies for capture, detection, and monitoring. Here, we report a class of hybrid optical sensing platforms based on poly(*N*-isopropylacrylamide-*co*-methacrylic acid) (pNIPAm-*co*-MAA) microgels interlaced with MIL-53(Al)-NH_2 metal–organic framework (MOF) nanoparticles for in situ sensing of dissolved CO_2 (dCO_2). Using an in situ hybridization strategy, MIL-53(Al)-NH_2 is uniformly embedded within the polymeric matrix, yielding microgel–MOF (M&M) hybrids with tunable porosity, optical responsiveness to dCO_2, and structural integrity controlled by the cross-linker. *N*,*N*′-Methylene-bis-acrylamide (BIS)-cross-linked M&M hybrid beads display greater rigidity, while poly(ethylene glycol)diacrylate (PEGDA)-cross-linked beads exhibit higher swelling ratios. Gas adsorption studies reveal reduced CO_2 uptake compared to pristine MIL-53(Al)-NH_2 MOF due to partial pore blocking by the polymer, yet the hybrid beads consistently outperform MOF-free ones, confirming that MIL-53(Al)-NH_2 remains functionally active within the microgel network. Ultraviolet–visible (UV–Vis) absorbance experiments highlight distinct hybrid behavior with dCO_2, inducing clear decreases in absorbance linked to MOF-mediated swelling, in contrast to the negligible response of pristine microgels. Reflectance spectroscopy further demonstrates that M&M-based etalons respond to dCO_2 through characteristic red shifts driven by MOF-mediated CO_2 adsorption and pore expansion, while MOF-free microgels show purely pH-driven blue shifts in response to dCO_2 due to the acidic environment. M&M beads with three different mass ratios between the microgel and the MOF are synthesized, among which the 5:1 hybrids with the BIS cross-linker exhibit the highest CO_2 uptake and deliver the most stable optical performance, maintaining reproducible responses over three consecutive CO_2 cycling tests. Notably, even the relatively low MOF loadings retained within the polymer matrix are sufficient to impart measurable CO_2 adsorption capacity and distinct optical responsiveness, underscoring the efficiency of the hybrid design. Our study establishes M&M etalons as dynamic, tunable platforms for real-time dCO_2 monitoring with potential applications in environmental and carbon capture technologies.

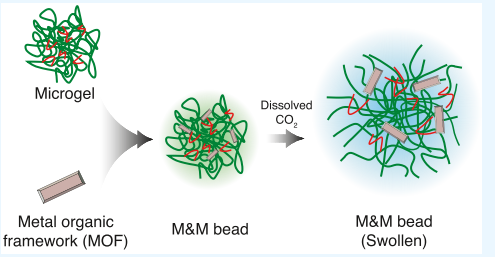

KEYWORDS: *stimuli-responsive microgels, metal–organic frameworks, hybrid materials, microgel–MOF etalons, dissolved CO_2 sensing*

INTRODUCTION

Carbon dioxide significantly impacts the world's oceans in addition to its effects on the atmosphere.[1] Ocean acidification refers to the decrease in seawater pH level caused by the oceans' continuous absorption of atmospheric CO_2.[2] This results in several chemical changes, including an increase in dissolved CO_2 (dCO_2), a drop in pH, and a decrease in the saturation levels of biologically significant calcium carbonate forms, such as aragonite and calcite.[3] Without substantial reductions in global CO_2 emissions, the structure of marine ecosystems is expected to change drastically.[4] Addressing this challenge requires accelerating the transition to renewable energy and developing negative emission technologies (NETs) to remove, store, or convert CO_2 into useful products. NETs include strategies for long-term storage or conversion, which rely on technological and natural methods to capture CO_2 either directly from the atmosphere or at emission points. Technological approaches include direct air capture (DAC) with geological storage and bioenergy with carbon capture and storage (BECCS), while natural methods comprise afforestation/reforestation and ocean-based methods such as alkalinity enhancement. A key component in many NETs is carbon capture and storage (CCS), which involves capturing CO_2 and storing it permanently underground.[5]

Among emerging approaches, Indirect Ocean Capture (IOC) is a hybrid technique that separates seawater into acidic and basic streams by removing atmospheric CO_2 through its equilibrium with seawater. In this process, CO_2 is released and collected as gas in the acid route and precipitates as solid calcium carbonate in the base route, enabling both gas capture and mineral storage. This process can produce high-

Received: November 3, 2025
Revised: December 24, 2025
Accepted: December 29, 2025
Published: January 7, 2026

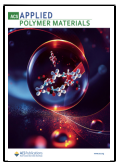

https://doi.org/10.1021/acsapm.5c04112
ACS Appl. Polym. Mater. 2026, 8, 1242–1257

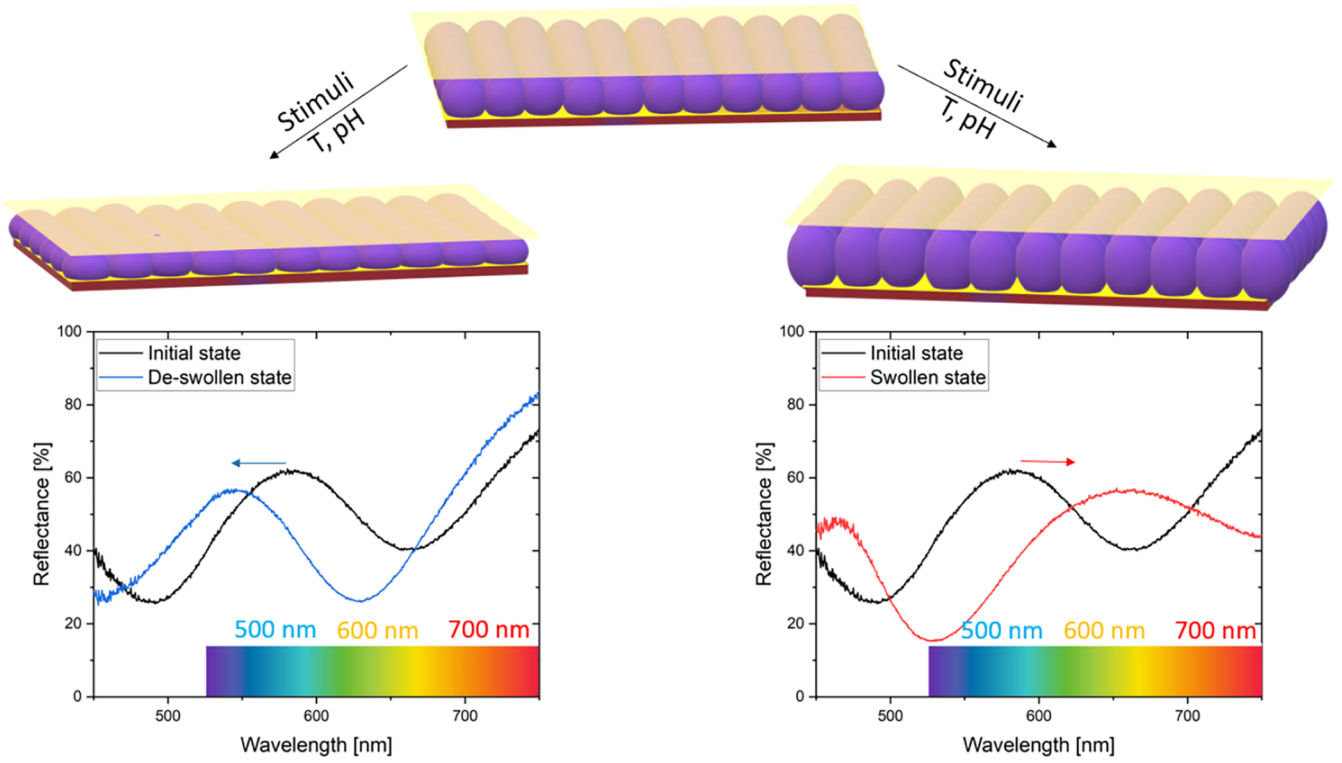

Figure 1. Schematic of microgel-based etalon response to external stimuli, leading to a peak shift in the reflectance spectrum.

purity CO_2 (up to 99%) and offers integration potential with desalination or power plants.[6] However, IOC remains at an early stage of development, and despite its promise, IOC lacks real-time, in situ sensing of key parameters such as pH and concentration of dCO_2, bicarbonate (HCO_3^-) and carbonate (CO_3^{2-}). Without continuous monitoring, it is difficult to track uptake efficiency or detect environmental risks such as localized acidification or alkalinization.[7]

Currently, most IOC prototypes rely on offline analysis, including total organic/inorganic carbon (TOC/TIC) analyzers, pH meters, flow meters, and pressure sensors, to monitor internal process dynamics. Laboratory measurements of pH, salinity, and alkalinity are often combined with modeling tools such as USGS CO_2Calc, a Seawater−Carbon Calculator developed by the U.S. Geological Survey, to indirectly estimate dissolved inorganic carbon (DIC).[8] While informative, these methods are not suitable for continuous, field-based deployment. Additionally, once treated seawater is reintroduced, it does not allow for environmental feedback, such as monitoring of local changes in pH, dCO_2 speciation, and biological responses.[9] Sensing dCO_2 in aqueous environments is an increasingly important challenge, with applications ranging from environmental monitoring to industrial process control. Integrating in situ sensing could greatly improve control, safety, and efficiency by enabling dynamic adjustments to acid/base dosing, while minimizing ecological impacts.[9,10] Hence, development of robust, responsive optical sensors could directly support the commercial deployment of IOC and similar technologies.

Stimuli-responsive optical sensing platforms, particularly microgel-based electrodes, offer a promising route to address this challenge. Microgel-based etalons have been fabricated for in situ sensing of a variety of stimuli, such as temperature, pH, and glucose, and have been used for several applications, such as environmental and chemical sensing of ionic strength and pH,[11,12] glucose monitoring,[13,14] protein detection[15] and development of functional membranes.[16,17] These devices consist of a dielectric microgel layer sandwiched between two reflective mirrors (often gold-coated), which selectively reflect light based on the distance between the mirror−mirror layer. The thickness of the microgel layer alters in response to stimuli, denoting the swelling/deswelling of the microgel beads. This, consequently, provokes a change in the mirror−mirror distance that determines the position and order of the peaks in the reflectance spectra.[18−20] Swelling is indicated by a redshift (longer wavelength), whereas deswelling yields a blueshift (shorter wavelength) in the reflectance spectra as shown in Figure 1.

Thermoresponsive poly(*N*-isopropylacrylamide) (pNIPAm) microgels are among the most studied systems for such applications.[20−24] A lower critical solution temperature (LCST) of about 32 °C governs the temperature-responsive behavior of pNIPAm-based microgels, at which they undergo volume phase transition (VPT).[25] Below the LCST, pNIPAm microgels exist in a swollen state due to strong hydrogen bonding between their hydrophilic segments and surrounding water molecules. Above the LCST, these hydrogen bonds weaken, causing water to be expelled from the cross-linked polymer network. As a result, the microgel particles collapse, transitioning into a deswollen state.[23,26] The network structure is maintained by cross-linkers, which form covalent bonds between polymer chains, enhancing mechanical integrity and enabling water retention.[27] For pNIPAm-based microgels, *N*,*N*'-methylenebis(acrylamide) (BIS) is a commonly used cross-linker,[11,28] producing microgels with greater compressive modulus and mechanical strength than alternative cross-linkers, such as, polyethylene glycol diacrylate (PEGDA) at equivalent degrees of cross-linking (DoC), making them more

https://doi.org/10.1021/acsapm.5c04112
ACS Appl. Polym. Mater. 2026, 8, 1242−1257

robust and rigid.[27,29] In contrast, PEGDA introduces hydrophilic, flexible PEG chains into the network, which increases water content and swelling capacity, further softening the microgel.[30] Such tunability in cross-linker chemistry allows optimization of mechanical and swelling properties for specific sensing environments.

pNIPAm microgels can be synthesized through various techniques, including free radical polymerization and precipitation polymerization.[31] Among these, precipitation polymerization is particularly effective for producing colloidal microgels with low polydispersity, tunable sizes, ranging from approximately 50 nm in the collapsed state to 1.5 μm in the swollen state, and controlled surface functionality.[18,28] Incorporating comonomers, small molecules, or proteins during synthesis allows for the development of multiresponsive microgels by altering their structural and functional properties. For example, incorporating methacrylic acid (MAA) as a comonomer imparts pH-responsiveness to thermoresponsive pNIPAm-based microgels.[32,33] At pH > pK_a of MAA ($\approx$ 4.65), the microgels are negatively charged, leading to the swollen state due to Coulombic repulsion between the negatively charged groups, while at pH < pK_a the MAA groups are protonated, and the microgels are in the deswollen state as a result of the lower electrostatic repulsion.[34,35]

An innovative approach is integrating metal−organic frameworks (MOFs) into the polymeric network of microgels. MOFs are crystalline, nanoporous solids consisting of metal ions or clusters linked by organic ligands, providing high surface area, tunable porosity, and diverse chemical functionalities.[36,37] These hybrid structures are excellent candidates for gas adsorption and separation technologies due to their high surface area and porosity, chemical functionality, and structural tunability. Their nanoporous architecture can be optimized to promote the selective adsorption of particular gases, such as CO_2.[38,39] Among them, MIL-53(Al)-NH_2 is a promising CO_2 adsorbent due to its amine-functionalized pore surfaces and its flexible pore structure, which enhances CO_2 capture via hydrogen bonding and acid−base interactions.[40] It is a member of the MIL-53 family and is composed of aluminum ions and aminoterephthalic acid as the organic linker. The amine groups use hydrogen bonds and acid−base interactions to improve CO_2 adsorption. Due to this unique property, MIL-53(Al)-NH_2 has been extensively studied for its high CO_2 adsorption capacity.[38,39,41,42]

Integrating porous crystalline materials, such as MOFs, with responsive polymeric systems has been developed for designing smart materials capable of sensing, separation, and adaptive behavior.[38,43−45] Among early contributions, functionalizing MOF nanoparticles via external-surface grafted polymers enables tunable functionality and colloidal behavior.[41,43,46,47] Thermoresponsive systems employing pNIPAm-tethered MOFs have also been emerged with applications spanning drug delivery, pollutant adsorption, and catalysis.[38,44,48,49,38,44,48,49] However, the successful and stable incorporation of MOFs into soft, water-dispersible microgels with well-controlled responsiveness remains a challenge.[48,50]

Here, we present a novel hybrid material consisting of pNIPAm-*co*-MAA microgels interlaced with MIL-53(Al)-NH_2, engineered into microgel−MOF(M&M)-based etalon structures for in situ detection of dCO_2. The innovation of our approach lies in an in situ hybridization strategy in which MIL-53(Al)-NH_2 nanoparticles are introduced during microgel synthesis. This process promotes intimate interlacing through weak electrostatic and hydrogen-bonding interactions between the MOF's amino groups and the microgel's carboxyl functionalities, ensuring uniform dispersion and strong interfacial compatibility. Comprehensive characterization, including particle size analysis, ζ-potential measurements, UV−Vis spectroscopy, and N_2/CO_2 adsorption, is used to confirm successful hybrid formation and assess structural properties. The resulting optical sensors are evaluated for responsiveness to various CO_2 speciations in water, namely, dCO_2, bicarbonate (represented by $NaHCO_3$), and carbonate (represented by Na_2CO_3), as well as a purely acidic environment (HCl). While dCO_2 exposure induces a pronounced red shift in the reflectance peak, HCl at comparable pH leads to a blue shift, confirming that the dCO_2 response arises from the MOF-mediated uptake rather than acidity alone. The (bi)carbonate speciations also yield red shifts under alkaline conditions, though distinct from the dCO_2 response. These hybrid etalons display reversible and reproducible optical shifts for up to three repeated dCO_2 cycling tests, demonstrating both durability and stability under operating conditions.

Our findings show that MOF-interlaced microgels can serve as highly tunable, stimuli-responsive platforms for real-time optical sensing of dCO_2 and (bi)carbonate speciations. By tailoring polymer−MOF interactions and preserving structural integrity, this approach enables advanced dCO_2 detection and broadens the scope of hybrid materials for capture, separation, and environmental monitoring applications. The ability of these hybrids to undergo predictable structural and optical changes in response to dCO_2 highlights their potential as dynamic components in next-generation smart sensing technologies. Integrating responsive, real-time sensing into CO_2 capture systems is essential to evaluate process efficiency, ensure operational stability, and minimize unintended environmental impacts while paving the way for more adaptive carbon management technologies.

EXPERIMENTAL SECTION

Materials

N,*N*′-Methylenebis(acrylamide) (BIS, ≥ 98.0%), poly(ethylene glycol)diacrylate (PEGDA, average M_n = 575, M_w = 302.00 g mol^{-1}), methacrylic acid (stabilized with MEHQ) (MAA, > 99.0%) and ammonium persulfate (APS, ≥ 98.0%) were all purchased from Sigma-Aldrich, The Netherlands and used as received. *N*-Isopropylacrylamide (NIPAM, 97%) was purified by recrystallization from hexanes (ACS reagent grade), both received from Sigma-Aldrich, The Netherlands. Hydrochloric acid (HCl) (ACS reagent, 37%), sodium bicarbonate ($NaHCO_3$) (ACS reagent, ≥ 99.7%), sodium carbonate (Na_2CO_3) (ACS reagent, ≥ 99.5%), aluminum nitrate nonahydrate ($Al(NO_3)_3{\cdot}9H_2O$, 99.9%), 2-aminoterephthalic acid (NH_2−BDC, 99%), nitric acid (HNO_3, 65%), acetone (ACS reagent, ≥ 99.5%), and *N*,*N*-dimethylformamide (DMF, 99.8%) were also obtained from Sigma-Aldrich, The Netherlands. Dry ice was purchased from Droogijs Shop, The Netherlands. All deionized (DI) water had a resistivity of 18.2 MΩ cm and was obtained from a Milli-Q Type 1 system from Merck KGaA, Germany.

Microgel Synthesis

Synthesis of poly(*N*-Isopropylacrylamide-*co*-methacrylic acid) (pNIPAm-*co*-MAA) microgels was performed via temperature ramp, surfactant-free, free radical precipitation polymerization as described previously.[20,38] In short, 1.358 g of the purified *N*-isopropylacrylamide (NIPAM) and 0.043 g (2.3 mol %) of *N*,*N*′-methylene-bis-acrylamide (BIS) were dissolved in 99 mL of Mili-Q water. The solution was filtered with 0.2 μm syringe filter and poured into a 250 mL three-

https://doi.org/10.1021/acsapm.5c04112
ACS Appl. Polym. Mater. 2026, 8, 1242−1257

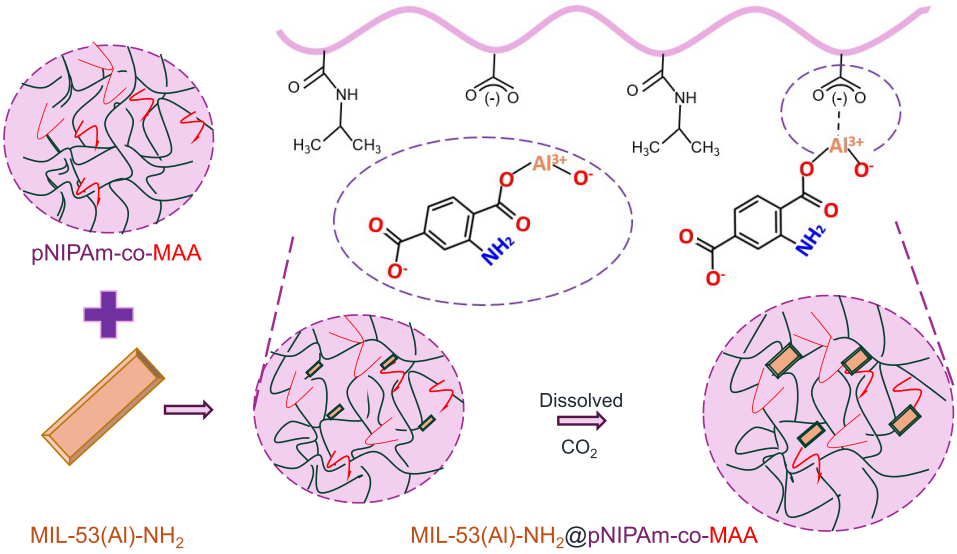

Figure 2. Schematic illustration of M&M hybrids formation. The response to dissolved CO_2 leads to a swollen state of M&M beads.

neck round-bottom flask, where it was heated under stirring to 70 °C for 1 h and purged with N_2. Once the temperature of the solution reached 70 °C, 0.146 mL of methacrylic acid (MAA) was added. 0.046 g of ammonium persulfate (APS) was dissolved in 1 mL of Mili-Q water and added to the solution to initiate the polymerization. The synthesis lasted 4 h and was performed in N_2 environment at 70 °C under stirring. The solution was filtered under vacuum and purified by centrifugation at 10,000 rpm for 1 h. The supernatant was removed from the pellet of particles, which were then resuspended with Mili-Q water. The procedure was performed six times to remove any unreacted monomer from the microgels.

pNIPAm-*co*-MAA microgels were synthesized with poly(ethylene glycol)diacrylate (PEGDA) as cross-linker. 1.358 g of NIPAM dissolved in 99 mL of Mili-Q water was mixed with 140 μL of PEGDA, corresponding to a NIPAm:PEGDA molar ratio of approximately 50:1 (2 mol % PEGDA). The rest of the synthesis procedure was performed identically as mentioned above for the BIS cross-linker.

MIL-53(Al)-NH_2 Synthesis

Synthesis of MIL-53(Al)-NH_2 was carried out under high pressure (>1 atm) and temperature (>100 °C) as described previously.[51] A 0.7602 g portion of aluminum nitrate ($Al(NO_3)_3{\cdot}9H_2O$) was dissolved in 5 mL of deionized (DI) water. Simultaneously, 0.5601 g of 2-aminoterephthalic acid (NH_2−BDC) was dissolved in 20 mL of N,N-dimethylformamide (DMF). The mixture was sealed in a 50 mL Teflon-lined stainless autoclave, which was heated up at 150 °C for 24 h, followed by spontaneous cooling down to room temperature. The precipitated sample was collected through centrifugal separation and washed thoroughly, 2 times with DMF and 1 time with DI water, before drying at room temperature overnight. The sample was transferred into a reflux with 140 mL DMF for boiling at 150 °C for 5 h. The product was washed 3 times with 30 mL of acetone and dried in a vacuum oven at 60 °C for 24 h. The sample was kept in the vacuum oven at 150 °C for another 24 h for activation.

Microgel-MIL-53(Al)-NH_2 Synthesis

MIL-53(Al)-NH_2 was dispersed in 20 mL of DI water after sonication for 30 min at room temperature by using a VWR USC-TH ultrasonic cleaner (VWR International, Radnor, PA) to ensure proper dispersion of MIL-53(Al)-NH_2 particles. After dissolving and filtering the mixture of NIPAm and BIS (or NIPAm and PEGDA) in 80 mL of DI water in a three-neck flask, the MIL-53(Al)-NH_2 suspension was filtered through a 0.2 μm syringe filter and placed in the same flask. The combined solution was then purged with nitrogen and subjected to the same heating (70 °C for 1 h) and polymerization conditions: MAA and APS were added to initiate polymerization, which was allowed to proceed for 4 h at 70 °C. The suspension was cooled overnight, filtered, and purified through multiple centrifugation and resuspension cycles as described for the standard microgel synthesis.

To evaluate the influence of MIL-53(Al)-NH_2 content on the hybrid material and to determine the optimal ratio for further synthesis, batches of 0.3 g, 0.194 and 0.136 g MIL-53(Al)-NH_2 were synthesized, using BIS as cross-linker, leading to M&M hybrids with 5:1, 8:1, and 10:1 microgel:MOF mass ratios. To evaluate the effect of the cross-linker on the hybrid material, a batch of 0.3 g MIL-53(Al)-NH_2 with PEGDA as the cross-linker was prepared, leading to the M&M mass ratio of 5:1 (Figure 2).

Microgel-MIL-53(Al)-NH_2 Etalon

The fabrication of the microgel-based etalon structure was similar to the previously reported procedure.[18,20] Briefly, a layer of 2 nm Cr and 15 nm Au was evaporated on 18 × 18 mm^2 glass substrates (Corning cover glasses) by physical vapor deposition (PVD) (CHA Industries, Inc., Solution PLC-S7). The gold-coated substrates were rinsed with ethanol, dried with a stream of N_2 gas, and placed on a hot plate at 30 °C for 5 min. On the gold-coated substrates, a uniform monolithic layer of pNIPAm-*co*-MAA-MIL-53(Al)-NH_2 or pNIPAm-*co*-MAA was created using the "paint-on" protocol.[18] A 40 μL aliquot of concentrated microgel or M&M dispersion was spread out toward the edges with a pipette tip. Spreading continued until the solution became too viscous. To ensure full drying, the coated substrate was heated to 35 °C for 2 h and subsequently rinsed with DI water to remove any unbound excess microgels from the Au layer. The sample remained on a hot plate at 30 °C overnight. A top layer of 2 nm Cr and 15 nm Au was subsequently evaporated on top of the dried monolithic layer to create the etalon structure. Based on our previously reported in-liquid AFM measurements, the thickness of the M&M film and Cr/Au top layer is estimated to be within the 400−560 nm range.[16]

Characterization Techniques

Dynamic Light Scattering (DLS). Dynamic Light Scattering (DLS) is performed to measure the particle size and the ζ-potential of the microgel and M&M suspensions. The Zetasizer Nano ZS, using a ZEN0112 and DTS1070 cuvette (Malvern Panalytical, U.K.), is employed for particle size and ζ-potential measurements, respectively. A volume fraction of 5.0% of the suspensions diluted in Milli-Q water is used. The particle size of the microgel beads is measured in the temperature range from 20 to 40 °C and from 40 °C back to 20 °C with an accuracy of ± 0.1 °C. The temperature cycle is intended to monitor both the swelling and deswelling of the microgel and evaluate the reversibility of its thermal transition. The swelling ratio

https://doi.org/10.1021/acsapm.5c04112
ACS Appl. Polym. Mater. 2026, 8, 1242−1257

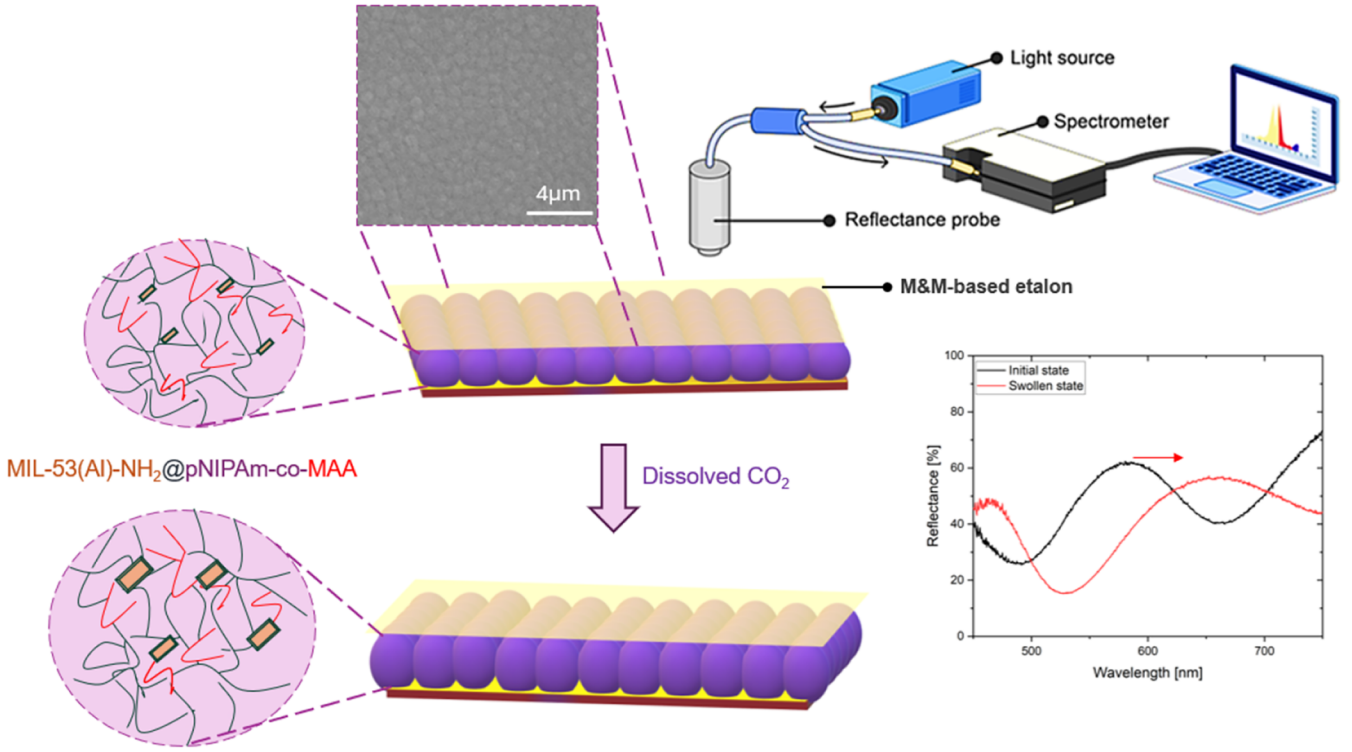

Figure 3. Schematic illustration of M&M-based etalon sensor, along with the SEM image of the monolithic layer of M&M beads (scale bar is 4 μm). The response to dissolved CO_2 leads to a peak shift that is detected by reflectance spectroscopy.

$$\text{swelling ratio} = \frac{d_{20^\circ\text{C (1st)}}}{d_{40^\circ\text{C (1st)}}} \quad (1)$$

in which $d_{20\ ^\circ\text{C (first)}}$ and $d_{40\ ^\circ\text{C (first)}}$ are the average hydrodynamic diameter of the microgel, respectively at the initial 20 °C measurement, and 40 °C at the end of the heating cycle, is calculated, showing stronger thermoresponsive shrinkage at higher ratios. The reversibility ratio

$$\text{reversibility ratio} = \frac{d_{20^\circ\text{C (2nd)}}}{d_{20^\circ\text{C (1st)}}} \quad (2)$$

was used to evaluate the reversibility of the temperature-induced volume transition. Where, $d_{20\ ^\circ\text{C (second)}}$ is the average hydrodynamic diameter after cooling back to 20 °C, and $d_{20\ ^\circ\text{C (1 st)}}$ is the initial value. The thermal swelling/deswelling cycle is fully reversible when the value is near 1. The ζ-potential is measured at temperatures of 20 and 40 °C with an accuracy of ± 0.1 °C. Each measurement is performed four times.

UV−vis Spectroscopy. The UV−vis absorbance is monitored to determine how the microgel and M&M respond to CO_2 in terms of swelling or deswelling. Measurements are carried out using a Shimadzu UV-1800 spectrophotometer (Shimadzu Corporation, Kyoto, Japan) over a wavelength range of 350−800 nm. Quartz cuvettes (Hellma Analytics SUPRASIL, type no. 104-QS, path length 10 mm) are used for all measurements. Different samples are examined as follows: (1) MOF-free microgels (BIS- and PEGDA-cross-linked), (2) M&M hybrids with BIS cross-linker at 5:1, 8:1, and 10:1 microgel:MOF ratios, and (3) PEGDA-cross-linked M&M composite at a 5:1 microgel/MOF ratio. In all samples, a volume fraction of 5.0% of the suspensions diluted in Milli-Q water is used. A cuvette with Milli-Q water is used for background correction for all spectra.

To introduce CO_2 into the samples, dry ice is used as the source of CO_2 gas. To prevent transfer-related variations, gas was directly bubbled into the open cuvette, including the sample, which was subsequently placed in the spectrometer. The UV−vis absorbance of each sample is measured before CO_2 bubbling, as well as within 5, 10, and 15 min of CO_2 bubbling. The pH of the samples is monitored during the experiments, observing a drop from 5.5 before CO_2 bubbling to 4.5 after 15 min of bubbling. This pH shift is consistent with the dissolution of CO_2 under ambient conditions, where the formation of carbonic acid lowers the pH into the mildly acidic regime. A final pH of ∼4.5 corresponds to the expected equilibrium of dissolved CO_2 and carbonate species at atmospheric pressure.[52,53]

Adsorption Behavior. N_2 and CO_2 adsorption of the MIL-53(Al)-NH_2, and the M&M samples cross-linked with BIS are measured using Tristar II (Micrometrics, The Netherlands). To perform the measurements, 100 mg of each sample is weighed. N_2 adsorption experiments are performed at −196 °C, and CO_2 adsorption at 25 °C. Prior to every measurement, the M&M samples are degassed for 10 h at 100 °C and the MIL-53(Al)-NH_2 for 15 h at 150 °C. An adsorption isotherm linear plot as a function of relative pressure is obtained for all samples after N_2 and CO_2 adsorption. For the latter, an isotherm linear plot as a function of absolute pressure is also provided.

Powder X-ray Diffraction (PXRD). The crystalline structure of MIL-53(Al)-NH_2 is detected with powder X-ray diffraction (PXRD) via a D8 ADVANCE diffractometer (Bruker, Germany).

Thermogravimetric Analysis (TGA). Thermogravimetric analysis (TGA) is performed to demonstrate the activation of the MIL-53(Al)-NH_2. TGA/SDTA851e thermogravimetric analyzer (Mettler Toledo, The Netherlands) is used under an air atmosphere with a flow rate of 100 mL/min. The sample mass is 6.1 mg, and the temperature is ramped from 30 to 800 °C at a constant heating rate of 5.00 °C/min. The sample stayed at 30 °C for 30 min before the temperature started to heat up.

Scanning Electron Microscopy (SEM). Scanning electron microscopy (JEOL 6010LA, Japan) is used to observe MIL-53(Al)-NH_2 MOF as well as the formation of the monolithic layer of the microgel-based and M&M-based etalons.

Inductively Coupled Plasma Mass Spectrometry (ICP-MS). Inductively coupled plasma mass spectrometry (ICP-MS) (ICP-MS Nexion 2000, PerkinElmer) is carried out to determine the concentration of aluminum (wt %) in the MIL-53(Al)-NH_2 and the

https://doi.org/10.1021/acsapm.5c04112
ACS Appl. Polym. Mater. 2026, 8, 1242−1257

M&M hybrids of 5:1 and 8:1 mass ratio to calculate the actual mass ratio of MOF in the M&M hybrids. Approximately 25 mg of the sample is dissolved in 1.5 mL of 65% HNO_3 and 4.5 mL of 30% HCl. After dissolution, the samples are diluted to 50 mL with Milli-Q water containing 1%HNO_3.

In Situ Detection of Microgel-Based Etalon Response

To detect the response of microgel-based etalons (with and without MOF) to the stimuli, namely, dCO_2, $NaHCO_3$, Na_2CO_3, and HCl solutions, in situ optical reflectance spectroscopy is performed. The microgel/M&M-based etalon is placed in a glass Petri dish, and a UV/vis reflectance probe (Ocean Optics, SR2 UV−vis, Florida) is placed on top of the etalon surface at an adjusted distance for optimal signal. To maintain consistency of the recorded spectra, the probe remains at the same position throughout each set of experiments. Once the etalon is immersed in the corresponding liquids, namely, DI water, $NaHCO_3$, Na_2CO_3, and HCl solutions, a spectrum is recorded by Ocean View 2.0.14 Software with a wavelength range of 400−750 nm (Figure 3).

Dry ice is used to bubble CO_2 gas into the glass Petri dish filled with DI water, where the etalon is immersed, to examine the etalon's response to dCO_2. This causes the pH to drop from 6.8 to 3.8 over a span of 45 min. The response of the M&M-based etalons to dCO_2 is studied over several cycles. Nitrogen gas (N_2) is bubbled through the solution to remove dCO_2 after each CO_2 exposure cycle, restoring the pH to its initial value of 6.8.[21] The etalon is able to regain its original optical state as a result of this regeneration. The reflectance measurement cycle is repeated on the same sample with new CO_2 exposure. Measurements are persisted until neither a blue shift nor a red shift is observed. To evaluate their response to (bi)carbonate speciations and pH, microgel-based and M&M-based etalons are immersed in $NaHCO_3$, Na_2CO_3, and HCl solutions, and the reflectance spectra are recorded in triplicate for each condition to ensure reproducibility.

RESULTS AND DISCUSSION

MOF and Microgel-MOF Hybrids

TGA, PXRD, and SEM analyses are conducted to verify the activation, crystallinity, and morphology of MIL-53(Al)-NH_2. TGA results (SI, Figure S1) confirm the absence of unreacted linkers or volatile impurities, indicating successful framework activation and good thermal stability. The crystalline structure of MIL-53(Al)-NH_2 is confirmed by PXRD. The X-ray powder diffraction pattern of the MIL-53(Al)-NH_2 is presented in the SI (see, Figure S2) and verifies the successful synthesis of MIL-53(Al)-NH_2, as the characteristic reflections are in agreement with reported literature patterns.[54,55] SEM imaging (SI, Figure S3) reveals that the MIL-53(Al)-NH_2 crystals exhibit a broad size distribution, with most particles ranging from 70 to 300 nm and a smaller fraction extending into the micrometer range. This nonuniformity likely reduces the amount of MIL-53(Al)-NH_2 introduced into the reaction flask during M&M synthesis, as larger particles were retained by the 0.2 μm syringe filter.

ICP analysis is employed to quantify the incorporation of MIL-53(Al)-NH_2 into the M&M hybrids. The Al content measured in the hybrids is markedly lower than expected from the feed ratios, indicating that only a small fraction of the MOF added during synthesis is retained in the polymeric network. While pristine MIL-53(Al)-NH_2 contains 20.7 wt % Al, the Al content of the 5:1 and 8:1 hybrids is determined to be 0.046 and 0.015 wt %, respectively (see SI, Table S1). This corresponds to approximately 1.4% and 0.7% retention of the initially added MOF, equivalent to ~2.22 mg and ~0.72 mg of MIL-53(Al)-NH_2 per gram of composite, respectively. Despite the relatively low incorporation efficiency, the retained MOF is sufficient to impart noticeable effects on UV−vis absorbance, gas adsorption behavior, and optical response to dCO_2, presented in the following sections, underscoring the strong influence of even small quantities of MIL-53(Al)-NH_2 within the hybrid matrix.

Dynamic Light Scattering (DLS)

Particle Size. Particle size measurements are performed to evaluate the effect of MOF incorporation on the thermoresponsive behavior of the microgels. M&M hybrids with different mass ratios and cross-linkers (BIS and PEGDA) as a function of temperature at pH 4.0, which is below the pK_a of MAA, are presented in Figure 4. Under these acidic conditions, carboxyl

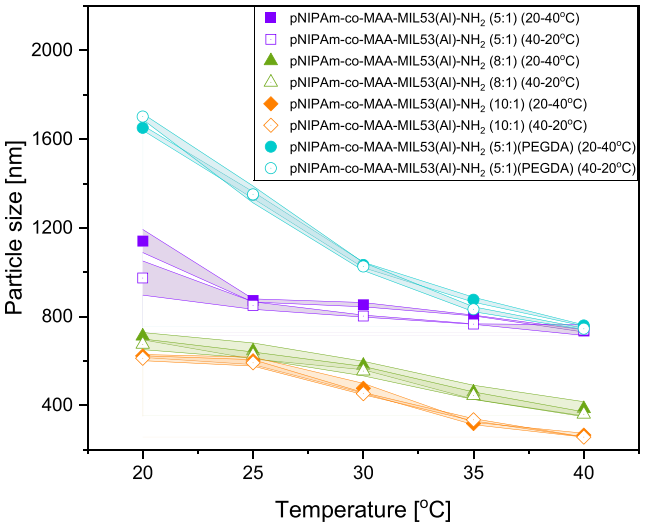

Figure 4. Particle size of microgel-MOF (M&M) hybrids with different mass ratios and cross-linkers as a function of temperature. Particle size of all the studied samples presents a standard deviation of ± 0.4 to ± 52.0 nm, with a total of three measurements at each temperature.

groups remain largely protonated, reducing electrostatic repulsion. At 20 °C, the initial particle size of BIS-cross-linked M&M hybrids increases with higher MOF content, indicating successful interlacing of the MOF into the polymer network. Particularly, 5:1 sample has a size of 1141 ± 52 nm, the 8:1 sample 711 ± 16 nm, and the 10:1 sample 622 ± 6 nm. The 8:1 sample consistently displays slightly larger particle sizes than the 10:1 sample, although both display comparable thermoresponsive behavior. The increase in the particle size with rising MOF content can be attributed to the presence of rigid MIL-53(Al)-NH_2 nanoparticles within the polymer network. Higher MOF loading introduces more inorganic domains that disrupt efficient polymer chain packing, leading to a more swollen structure, expanding the microgel's hydrodynamic volume.[56] In contrast, the 5:1 sample demonstrates a more pronounced size increase at low temperature, suggesting that excessive MOF loading may hinder structural flexibility and partially interfere with the thermoresponsive swelling behavior or promote partial aggregation within the network. The MOF-loaded PEGDA sample remains consistently larger than the MOF-loaded BIS sample, a result attributed to the lower effective cross-linking density of PEGDA compared to BIS.[57,58] The higher swelling ratios observed for PEGDA-based M&M hybrids stem from their significantly larger particle size at 20 °C, while both

https://doi.org/10.1021/acsapm.5c04112
ACS Appl. Polym. Mater. 2026, 8, 1242−1257

Table 1. Swelling and Reversibility Ratios of Microgel and Microgel−MOF Samples with Standard Deviations

Sample	Swelling ratio	Reversibility ratio
pNIPAm-co-MAA (BIS)	1.91 ± 0.10	0.98 ± 0.02
pNIPAm-co-MAA (PEGDA)	2.47 ± 0.11	0.94 ± 0.06
pNIPAm-co-MAA-MIL-53(Al)-NH_2 (5:1) (BIS)	1.53 ± 0.06	0.77 ± 0.08
pNIPAm-co-MAA-MIL-53(Al)-NH_2 (8:1) (BIS)	1.98 ± 0.13	0.95 ± 0.05
pNIPAm-co-MAA-MIL-53(Al)-NH_2 (10:1) (BIS)	2.43 ± 0.11	0.98 ± 0.03
pNIPAm-co-MAA-MIL-53(Al)-NH_2 (5:1) (PEGDA)	2.24 ± 0.08	1.03 ± 0.03

PEGDA and BIS systems converge to similar sizes upon deswelling at 40 °C.

Swelling and reversibility ratios for all systems are summarized in Table 1. The swelling ratios, ranging between 1.5 and 2.5 in diameter, confirm strong thermo-responsivity and are consistent with typical values reported in literature (approximately 1.6 to 2.2).[59] Reversibility ratios close to unity (0.94 to 1.03) further indicate excellent cyclic stability, with the exception of the BIS-cross-linked M&M (5:1) system, which shows a noticeably reduced reversibility ratio of 0.77. This suggests partial structural irreversibility, most likely caused by MOF incorporation and the partial release of MOF from the polymer matrix during the cooling cycle. MIL-53(Al)-NH_2 is likely interacting through weak electrostatic interactions with the carboxyl groups of MAA or the amide groups of PNIPAm, consistent with studies showing that weak electrostatic and hydrogen-bonding interactions between MOF surface functional groups and polymer carboxyl/amide moieties govern interfacial binding in MOF−polymer hybrids.[60−62] During thermal cycling, these relatively weak interactions may not be sufficient to permanently anchor the MOF within the microgel framework, and the release of MOF is therefore likely governed by physical expulsion from the shrinking network upon deswelling. To address this limitation, the 5:1 system was resynthesized using PEGDA as a cross-linker. The PEGDA-based hybrid exhibited full reversibility and a higher swelling ratio, underscoring the critical role of cross-linker chemistry in dictating thermal response, structural integrity, and retention of MOFs in M&M hybrids. Notably, the PEGDA-cross-linked M&M (5:1) hybrid exhibits superior reversibility compared to its BIS-based counterpart. This arises from the flexible and hydrophilic PEGDA chains that yield a softer, more elastic network capable of accommodating repeated swelling/deswelling without structural fatigue, unlike the more brittle BIS-cross-linked framework.[57,58] For PEGDA-cross-linked systems (see SI, Figures S4 and S5(b), for comparison between pristine microgel using BIS and PEGDA as cross-linker and between pristine microgel and 5:1 ratio of microgel-MOF, using PEGDA as cross-linker, respectively), both the pristine microgel and its 5:1 MOF hybrid show high swelling ratios and excellent reversibility Table 1).

ζ-Potential. Surface charge, reflected in the ζ-potential, is primarily governed by deprotonation of the carboxyl group of MAA ($-COO^-$) in pNIPAm-co-MAA microgels. The ζ-potentials of both the pristine microgels and the M&M hybrids cross-linked with BIS and PEGDA are measured at 20 and 40 °C and pH 4.0 (Figure 5, see SI, Table S2, for the values and the standard deviation of each sample). At elevated temperatures, deswelling of beads leads to the concentration of $-COO^-$ groups near the particle surface, increasing ion mobility, which leads to more negative ζ-potential values. PEGDA-cross-linked microgels exhibit less negative values compared to their BIS-cross-linked counterparts, consistent

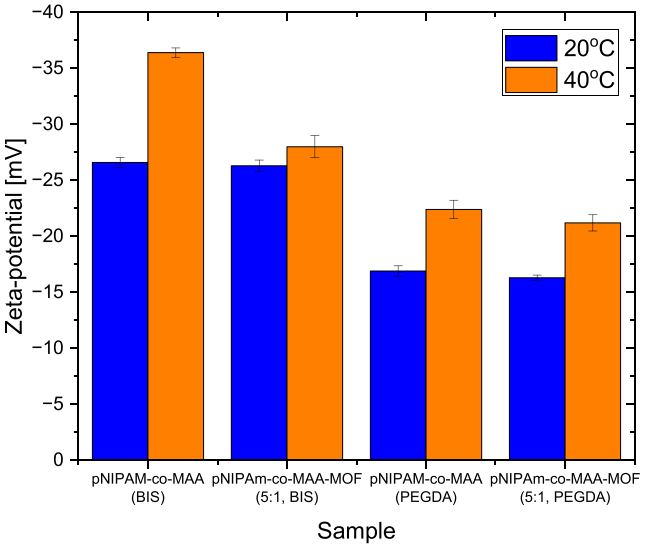

Figure 5. ζ-potential of microgels and microgel-MOF (M&M) hybrids with BIS and PEGDA as cross-linkers at 20 and 40 °C. The ζ-potential of all the studied samples presents a standard deviation of ± 0.23 to ± 0.99 mV, with a total of four measurements at each temperature.

with the less ionic nature of PEGDA.[63,64] Upon incorporation of MIL-53(Al)-NH_2, only a slight decrease in ζ-potential is observed at 20 °C, while at 40 °C the hybrids display less negative values compared to the pristine microgels (see SI, Figure S6, for comparison between different ratios of microgel-MOF, namely, 5:1, 8:1, and 10:1 using BIS as the cross-linker). This trend can be attributed to the positively charged Al^{3+} metal nodes and $-NH_2$ functionalities of the MOF, which partially neutralize the negatively charged $-COO^-$ groups of MAA. The reduced negativity further confirms the successful interlacing of MIL-53(Al)-NH_2 within the microgel matrix. Importantly, the overall ζ-potential remains negative, ensuring that the hybrid systems maintain a colloidal stability.

For PEGDA-cross-linked systems, a smaller temperature-induced difference is observed between the pristine microgels and the corresponding M&M hybrids. This behavior denotes that PEGDA-based networks provide a more uniform distribution of charge and weaker electrostatic interactions with the MOF, resulting in a reduced sensitivity of the surface charge to thermal deswelling. Consequently, PEGDA-cross-linked hybrids may offer improved stability under fluctuating temperature conditions compared to their BIS counterparts.

UV−Vis Absorbance

UV−Vis spectroscopy is employed to monitor the optical response of microgel and M&M hybrids during CO_2 bubbling. According to the Beer−Lambert law

$$A = \varepsilon c d \tag{3}$$

https://doi.org/10.1021/acsapm.5c04112
ACS Appl. Polym. Mater. 2026, 8, 1242−1257

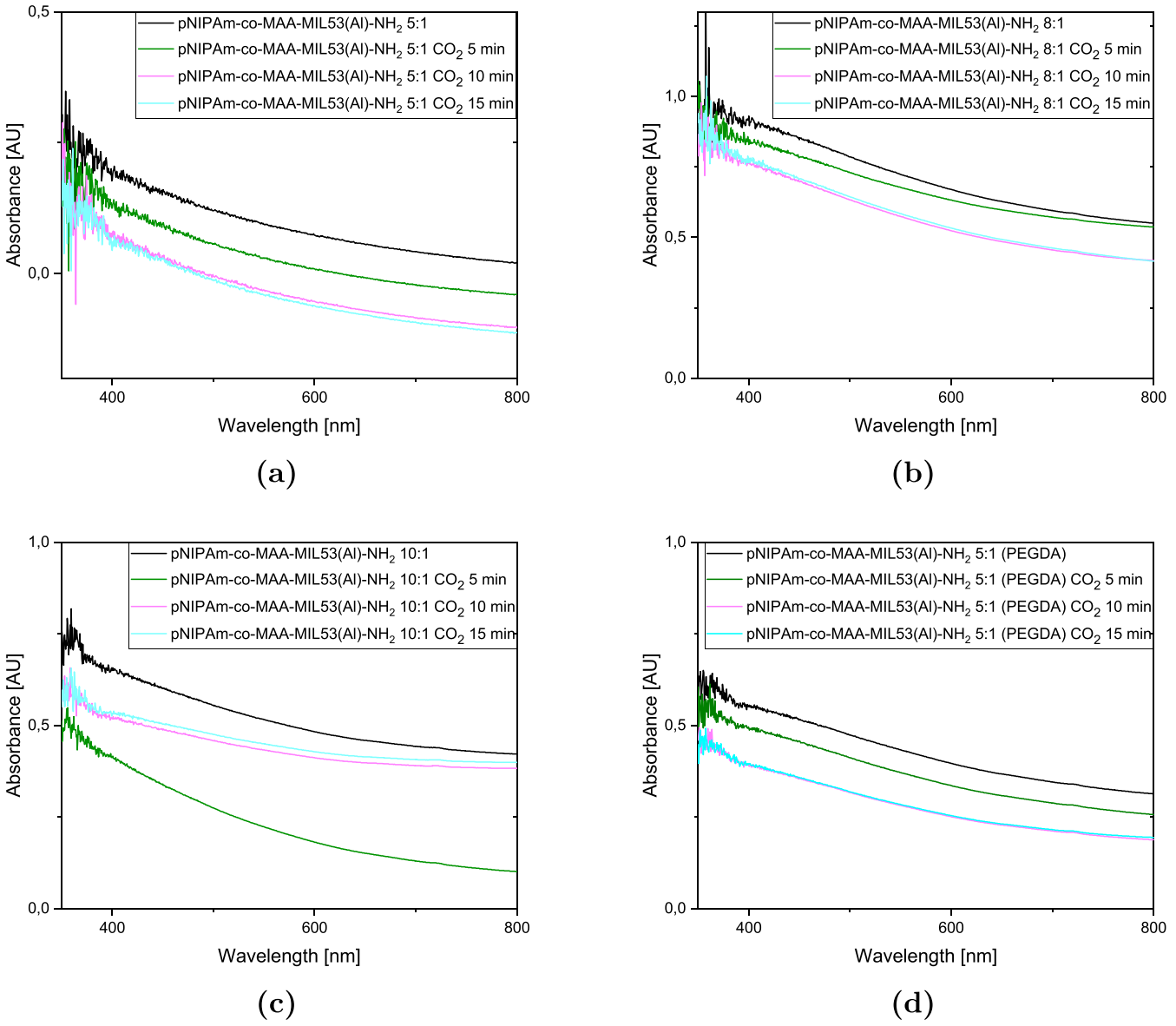

Figure 6. UV−VIS spectroscopy measurements of Microgel−MOF hybrids with BIS as cross-linker with mass ratios of: (a) 5:1, (b) 8:1, (c) 10:1, and (d) 5:1 ratio with PEGDA as the cross-linker.

absorbance (A) depends on the optical path length (d), the molar absorptivity (ε), and the concentration of absorbing or scattering species within the medium (c).

In colloidal microgel systems, swelling increases the water content and decreases the particle refractive index contrast relative to the solvent, leading to a reduction of light scattering and lowering the measured absorbance. Deswelling leads to denser particles with higher refractive index contrast, resulting in greater light scattering and increased absorbance.[31,65,66] Hence, a decrease in absorbance is anticipated if CO_2 adsorption causes microgels to swell, and an increase in absorbance would indicate deswelling of the microgels as response to the pH drop caused by dCO_2.

The MOF-free BIS and PEGDA microgels (SI, Figure S7) exhibit no discernible change in absorbance after 5 min of CO_2 bubbling, indicating negligible CO_2 adsorption and no measurable pH-triggered volume transition. A slight increase in absorbance is observed after 10 and 15 min, affirming the deswelling response of the microgel beads to the pH drop caused by dCO_2.

For the BIS-cross-linked M&M hybrids, distinct absorbance changes are observed for different microgel-MOF ratios (Figure 6(a,b,c)). The 5:1 system shows a clear drop in absorbance after 5 and 10 min of bubbling with minimal change between 10 and 15 min, suggesting rapid CO_2 uptake followed by saturation. The 8:1 system also displays a gradual decrease in absorbance, with a smaller shift between 0−5 min and a more pronounced shift between 5−10 min, consistent with slower adsorption kinetics due to reduced MOF content. In contrast, the 10:1 system exhibits a sharp decrease in absorbance within the first 5 min—greater than that of the 5:1 and 8:1 samples, indicating rapid CO_2 uptake. This is, however, followed by an unexpected increase after 10 min, implying partial deswelling and reduced stability, making it less suitable for sustained CO_2 adsorption.

The PEGDA-cross-linked M&M hybrids at a 5:1 ratio (Figure 6(d)) display a response pattern closely resembling

https://doi.org/10.1021/acsapm.5c04112
ACS Appl. Polym. Mater. 2026, 8, 1242−1257

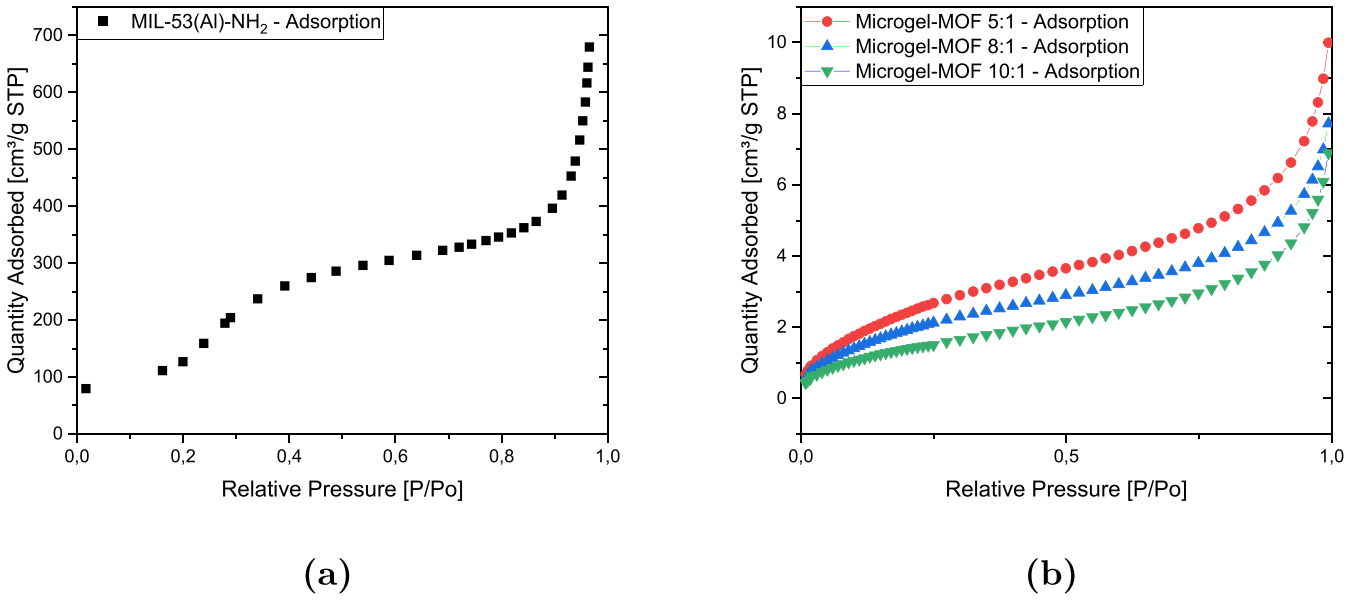

Figure 7. Isotherm linear plot of N_2 adsorption for: (a) MIL-53(Al)-NH_2 and (b) microgel-MIL-53(Al)-NH_2 in 5:1, 8:1 and 10:1 mass ratios.

that of the BIS-cross-linked 5:1 sample, showing a similar trend in absorbance decrease over the 0−5 min and 5−10 min intervals, and no further change between 10−15 min. These results indicate that cross-linker type has no significant influence on CO_2 adsorption under the tested conditions. Overall, UV−vis analysis suggests that a 5:1 microgel:MOF ratio provides the most consistent and efficient CO_2 uptake performance, regardless of the type of cross-linker.

The observed decrease in absorbance upon CO_2 exposure in the responsive M&M systems is consistent with well-established optical behavior of thermoresponsive microgels. In the swollen state, water uptake lowers the effective refractive index of the microgel network, reducing light scattering and shifting the optical band to shorter wavelengths, which results in a lower absorbance index (eq 3). Swelling produces a blue shift, while deswelling/collapse yields a red shift due to increased refractive index contrast. Consequently, this links lower absorbance values to the swollen, water-rich state.[67−69] Collectively, these findings support the interpretation that the absorbance drop in our CO_2-responsive systems originates from CO_2-induced swelling of the M&M network due to CO_2 adsorption into the MOF pore structure. The adsorbed CO_2 is primarily confined within the porous MIL-53(Al)-NH_2 domains, promoting local water uptake and expansion of the surrounding microgel matrix. Upon prolonged CO_2 bubbling, the adsorption capacity of the MOF becomes saturated, and additional CO_2 dissolves in water, lowering the pH of the medium. This acidification protonates the carboxyl groups of the polymer network, leading to microgel deswelling and a gradual increase in absorbance.

Adsorption Behavior

N_2 Adsorption. The N_2 adsorption isotherm of pristine MIL-53(Al)-NH_2 and M&M hybrids as a function of relative pressure (P/P_o) is presented in Figure 7, where P_o is the saturation vapor pressure of nitrogen at the measurement temperature. The nitrogen adsorption isotherm of pristine MIL-53(Al)-NH_2 (Figure 7(a)) exhibits a typical Type I/IV behavior, indicative of a microporous framework with some mesoporosity, consistent with previous reports on MIL-53(Al)-NH_2.[55,70] Type I isotherms reflect gas uptake in narrow pores (<2 nm), while Type IV features arise from capillary condensation in mesopores (2−50 nm).[71] The adsorbed quantity increases sharply at low relative pressures (P/P_o < 0.1), reflecting the high affinity of CO_2-philic pores for N_2 and the presence of micropores (<2 nm). The gradual increase at higher pressure ratios (P/P_o > 0.8) shows multilayer adsorption and potential pore expansion or interparticle mesoporosity. The steep uptake in the relative pressure region of 0.9−1.0 suggests the presence of interparticle voids associated with the packing of MOF nanoparticles (see SEM images in SI, Figure S3), which provide additional textural porosity beyond the intrinsic microporous framework.[72,73]

Upon incorporation of MIL-53(Al)-NH_2 into pNIPAm-co-MAA microgels to form hybrid composites at mass ratios of 5:1, 8:1, and 10:1, a significant reduction in nitrogen uptake is observed for all M&M hybrids (Figure 7(b)). This decrease is particularly pronounced at low relative pressures, indicating that a substantial fraction of the MOF's micropores is either physically occluded by the polymer network or partially blocked due to embedding within the hydrated microgel matrix, which remains in a swollen state below the LCST. The gradual increase in adsorption at higher relative pressures across all M&M hybrids indicates the presence of additional mesoporosity arising from the interstitial spaces between microgel beads or the swelling-induced porosity of the polymer network.[74] This effect is more prominent in the 5:1 system, consistent with the higher MOF content and greater contribution of interfacial voids. Among the hybrids, the 5:1 M&M system exhibits the highest nitrogen uptake, suggesting that higher MOF loading allows for more accessible pore volume within the hybrid, while the 10:1 system shows the lowest adsorption, reflecting a lower absolute MOF content and/or more restricted pore accessibility due to polymer coverage.

Interestingly, using the aluminum content determined by ICP (see SI, Table S1), the amount of MIL-53(Al)-NH_2 incorporated into the 5:1 and 8:1 hybrids corresponds to only 0.22 and 0.07 wt %, respectively. This would theoretically

https://doi.org/10.1021/acsapm.5c04112
ACS Appl. Polym. Mater. 2026, 8, 1242−1257

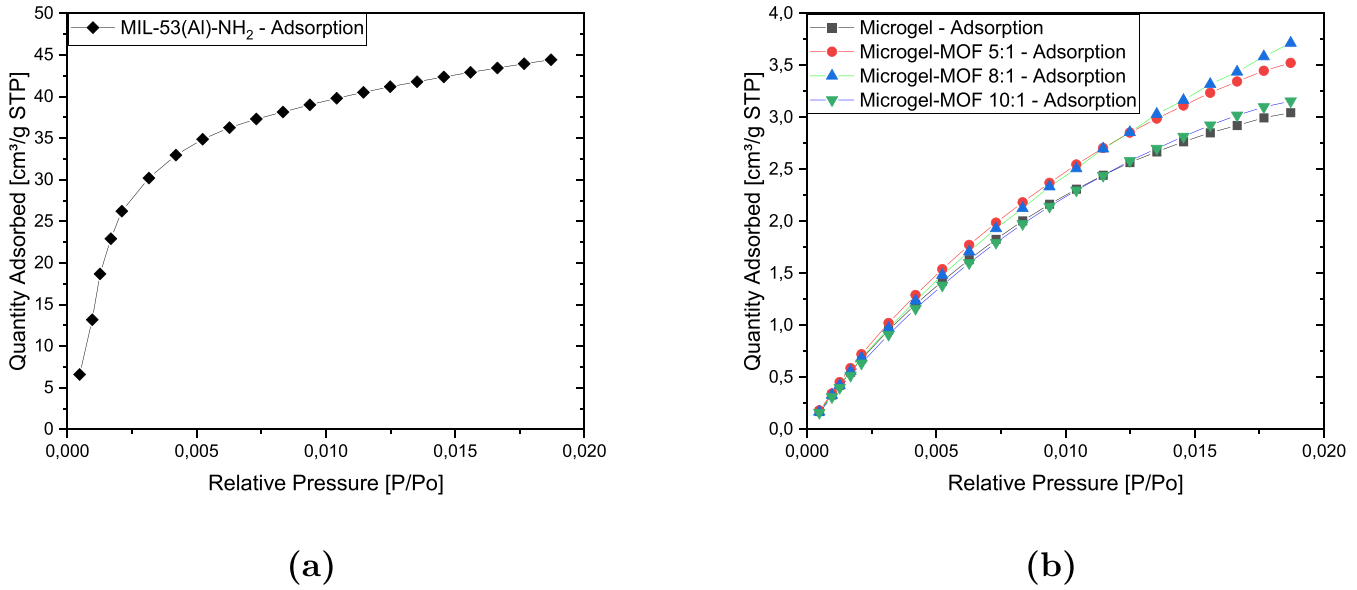

Figure 8. Isotherm linear plot of CO_2 adsorption for: (a) MIL-53(Al)-NH_2 and (b) microgel and microgel-MIL-53(Al)-NH_2 in 5:1, 8:1 and 10:1 mass ratios.

contribute to 1.30 and 0.42 cm^3/g STP of N_2 adsorption based on the uptake of pristine MIL-53(Al)-NH_2 (583 cm^3/g STP at P/P_o = 0.95, see Figure 7(a))(see SI, N_2 and CO_2 adsorption for calculations). However, the measured N_2 uptakes of the 5:1 and 8:1 hybrids at P/P_o = 0.95, namely 7.78 and 6.14 cm^3/g STP, respectively (see Figure 7(b)), exceed these theoretical values by more than an order of magnitude. These results demonstrate that while embedding MIL-53(Al)-NH_2 into microgels reduces the absolute nitrogen uptake relative to the pristine MOF, the hybrids retain accessible porosity that can contribute to gas adsorption. The trend observed across different mass ratios confirms the role of MOF loading in tuning the accessible pore volume and highlights the trade-off between polymer encapsulation and MOF availability in designing responsive M&M hybrids.

CO_2 Adsorption. The CO_2 adsorption isotherm of pristine MIL-53(Al)-NH_2 and M&M hybrids as a function of relative pressure (P/P_o) is presented in Figure 8(a), and as a function of absolute pressure (kPa) is presented in the SI (see, Figure S8). The CO_2 adsorption isotherm of pristine MIL-53(Al)-NH_2 shows a steep uptake at low relative pressures (P/P_o < 0.01), characteristic of a highly microporous framework with strong affinity toward CO_2. This behavior is consistent with the well-documented breathing effect of MIL-53(Al)-NH_2, where the flexible framework undergoes structural changes between narrow-pore (np) and large-pore (lp) forms, enhancing CO_2 capture through both physisorption and framework interactions.[55,75] The high adsorbed quantity (>40 $cm^3\ g^{-1}$ STP) underscores the intrinsic porosity and open pore accessibility of the MOF.

The microgel−MIL-53(Al)-NH_2 hybrids (Figure 8(b)) exhibit markedly reduced CO_2 adsorption capacities, with values in the range of 3.0−3.8 $cm^3\ g^{-1}$ STP. This reduction is potentially due to the encapsulation of MOF particles within the polymeric microgel matrix, which introduces diffusion limitations and partially blocks access to the intrinsic micropores of MIL-53(Al)-NH_2.[74,76] The polymer chains likely act as a barrier to gas transport, and swelling/deswelling dynamics may further hinder adsorption at low pressures, in line with previous findings on MOF−polymer hybrids.[77,78]

The effect of the MOF on the polymer network is clearly noticeable. The hybrids consistently show higher CO_2 uptake compared to the pure microgel, confirming that even when partially confined, MIL-53(Al)-NH_2 provides additional porosity, enhancing gas sorption properties of the microgel network. This indicates that the MOF particles retain functional activity within the polymeric framework and are not completely encapsulated or inaccessible.

Among the hybrid systems, the 5:1 mass ratio exhibits the highest CO_2 uptake compared to that of 8:1 and 10:1. This can be explained based on the larger amount of incorporated MOF relative to polymer, leading to greater accessible porosity. Particularly, based on the ICP-derived Al values (wt%) (see SI, Table S1), the actual MIL-53(Al)-NH_2 content in the hybrids corresponds to 0.22 wt % for 5:1 hybrids and 0.07 wt % for 8:1 hybrids. Using a CO_2 uptake of 44 cm^3/g STP for pristine MIL-53(Al)-NH_2 at P/P_o = 0.018 (see Figure 8(a)) and assuming that gas uptake scales linearly with the MOF content, the expected CO_2 adsorption capacities would be 0.10 and 0.03 cm^3/g STP, respectively (see SI, N_2, and CO_2 adsorption for calculations). The experimentally measured values are, however, 3.52 and 3.42 cm^3/g of STP at P/P_o = 0.018 for 5:1 and 8:1 hybrids, respectively (see Figure 8(b)). This large discrepancy demonstrates that the polymer network itself contributes significantly to CO_2 adsorption and further disruption of polymer chain packing and creation of interfacial free volume induced by MOF incorporation, enhancing adsorption beyond what is predicted based on its low loading.[61,79] The 8:1 hybrid shows an intermediate adsorption capacity, while the 10:1 system displays the lowest uptake, which may reflect both the reduced MOF content and stronger confinement by the microgel network. The slight improvement of the 8:1 system over 10:1 further suggests that the optimal balance between the MOF loading and polymer confinement is crucial for maintaining accessible porosity.

The above highlights the trade-off between the high CO_2 capacity of MIL-53(Al)-NH_2 and the stabilization/diffusion

https://doi.org/10.1021/acsapm.5c04112
ACS Appl. Polym. Mater. 2026, 8, 1242−1257

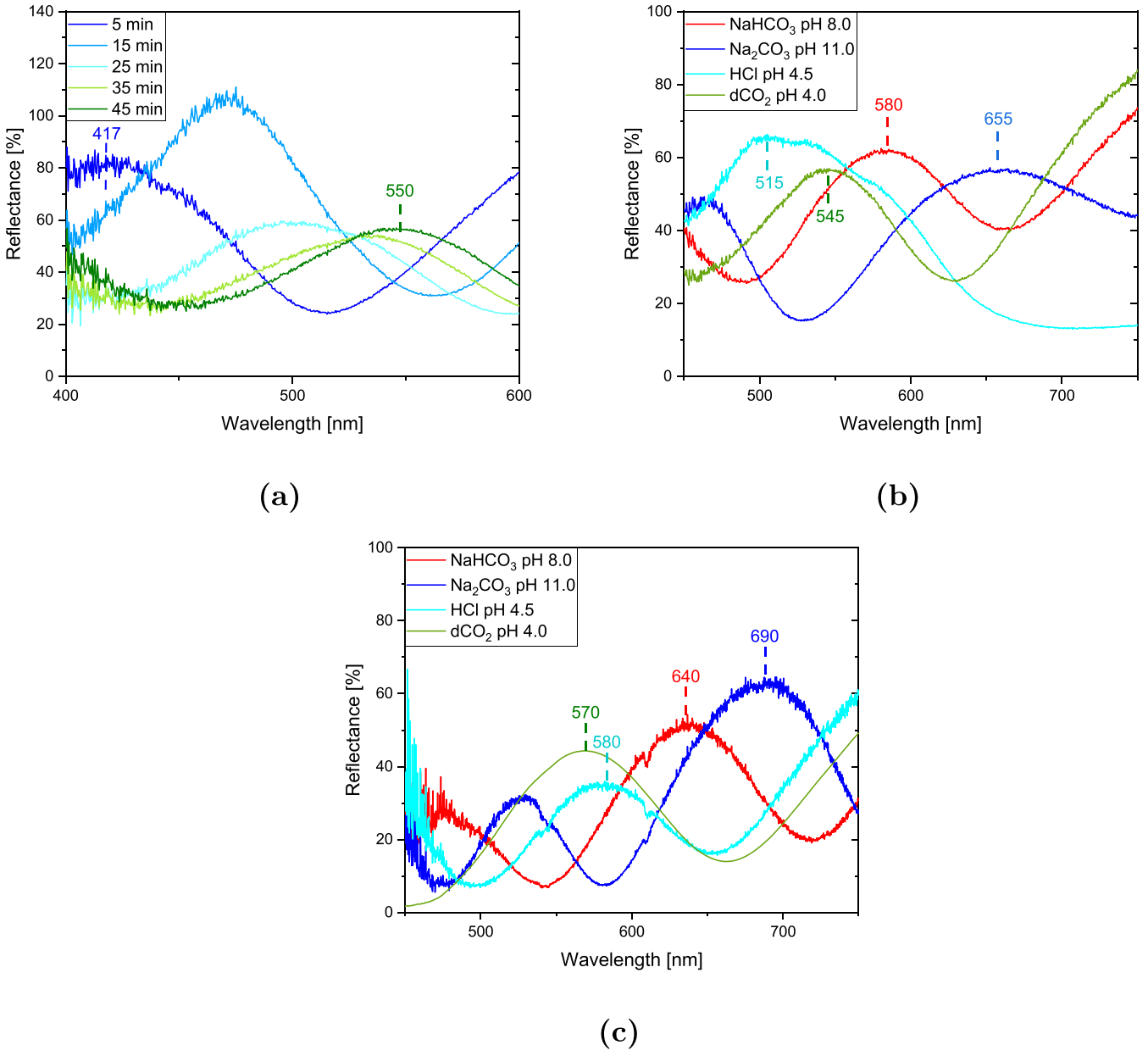

Figure 9. Reflectance spectrum of: (a) microgel-MOF (M&M) based etalon with 5:1 mass ratio upon response to dCO_2 as a function of time, (b) microgel-MOF (M&M) based etalon with 5:1 mass ratio as response to $NaHCO_3$, Na_2CO_3, HCl, and dCO_2, and (c) microgel-based etalon as response to $NaHCO_3$, Na_2CO_3, HCl, and dCO_2.

control imparted by the microgel matrix. Incorporation of the MOF into the polymer network reduces accessible porosity due to partial pore blocking and limited gas diffusion through the hydrated polymer environment. This confinement introduces reversible, stimuli-responsive behavior resulting in the hybrid structure that represents a balance between maximized sorption performance and controlled, tunable accessibility. This trade-off provides a pathway for designing stimuli-responsive CO_2 sensors, where swelling/deswelling behavior modulates accessibility, coupling molecular adsorption with measurable optical responses.

In Situ Response of M&M-Based Etalons to CO_2

Reflectance spectroscopy is performed to evaluate the response of the M&M-based etalons to dCO_2 (Figure 3). Figure 9(a) presents the response of the 5:1 M&M-based etalon. The M&M-based etalon is exposed to dCO_2 for 5 min and at t = 5 min, the maximum reflectance peak is observed at λ_{max} = 417 nm. With continuous CO_2 bubbling, a progressive red shift is detected, consistent with the swelling of the hybrid beads, until saturation is reached at 45 min (λ_{max} = 550 nm). Beyond this point, no further shift is observed, indicating that the M&M layer has reached its adsorption capacity. The markedly shorter equilibration time observed in the UV−Vis experiments (10 min) compared to reflectance spectroscopy (45 min) can be attributed primarily to differences in sample configuration and CO_2 transport dynamics. During UV−vis, CO_2 is directly bubbled into dilute M&M suspensions, where rapid gas dissolution and diffusion throughout the dispersed particles enable fast equilibration. In contrast, the reflectance measurements are performed on M&M-based etalons, where hybrid microgel particles form a densely packed film with larger

https://doi.org/10.1021/acsapm.5c04112
ACS Appl. Polym. Mater. 2026, 8, 1242−1257

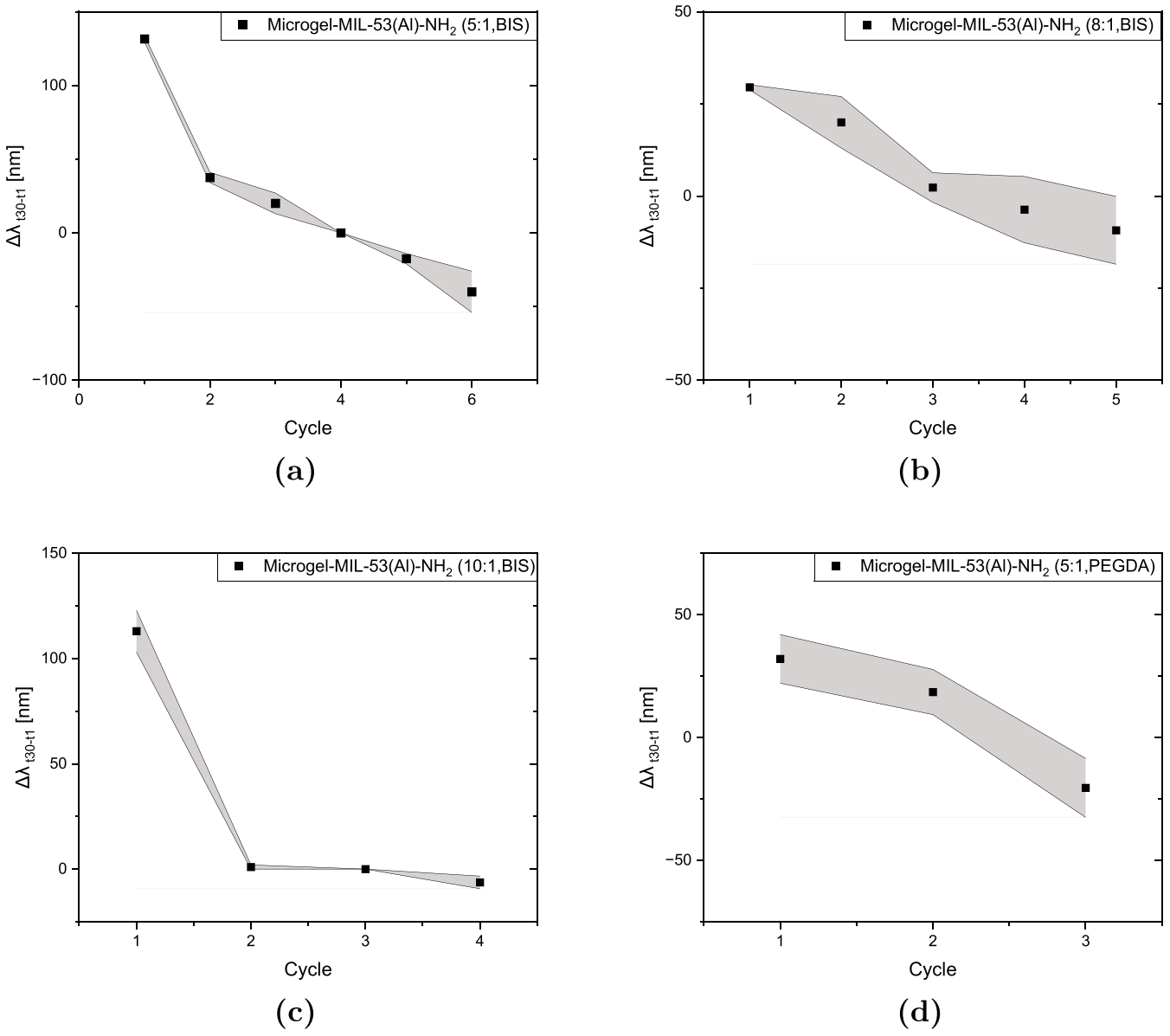

Figure 10. Average peak shift of the microgel-MOF (M&M) based etalon sensor in dissolved CO_2 (dCO_2) during several cycles (shaded region shows the standard deviation obtained from three samples). $\Delta\lambda_{t30\text{-}t1}$ per cycle of: (a) 5:1 mass ratio, (b) 8:1 ratio, (c) 10:1 ratio, and (d) 5:1 ratio with PEGDA as cross-linker. The positive values of $\Delta\lambda$ demonstrate the red shift due to the swelling of the M&M hybrids in response to dCO_2. The negative values of $\Delta\lambda$ demonstrate the blue shift due to the deswelling of the M&M hybrids as a response to acidification induced by dCO_2.

interfacial area but longer diffusion paths for CO_2, causing slower gas penetration and longer time to reach saturation.

During the experiment, the pH of the DI water decreased from 6.0 at 5 min to 4.0 at 45 min. The acidification of the DI water, induced by CO_2 dissolution at room temperature and atmospheric pressure, denotes the saturation point when the pH reaches 4.0.[52,53] In principle, low pH conditions typically induce microgel deswelling, observed as a blue shift in reflectance spectra.[11,16] The red shift obtained here reinforces the notion that the swelling response of the hybrid system arises from the capture of CO_2 within the porous cavities of the MOF, rather than from pH alone. This response originates from physical interactions between dissolved CO_2 and the hybrid network. CO_2 uptake occurs through physisorption within the MOF cavities and reversible structural rearrangement of the microgel−MOF layer. No chemical reaction takes place between CO_2 and the polymer or the MOF, and therefore, no additional chemical species or reaction by-products are formed during the process.

To further assess this mechanism and the response to different CO_2 speciations and pH, the M&M-based etalon (5:1) is immersed in $NaHCO_3$, Na_2CO_3, and HCl solutions, and the corresponding spectral response is compared to that observed under dCO_2 bubbling (Figure 9(b)). Compared to the etalon response to dCO_2 ($\lambda_{max,\ pH\ 4.0}$ = 545 nm), a red shift is observed under basic conditions, consistent with the swollen state of the hybrid beads: $\lambda_{max,pH\ 8.0}$ = 580 nm at pH 8.0 ($NaHCO_3$) and $\lambda_{max,pH\ 11.0}$ = 655 nm at pH 11.0 (Na_2CO_3). In contrast, immersion in HCl at pH 4.5 produces a blue shift ($\lambda_{max,pH\ 4.5}$ = 515 nm), reflecting the deswollen state of the microgels under acidic conditions. Interestingly, when exposed to dCO_2 at pH 4.0 for 45 min, the M&M-based etalon exhibits a red shift ($\lambda_{max,\ pH\ 4.0}$ = 545 nm). This divergence

https://doi.org/10.1021/acsapm.5c04112
ACS Appl. Polym. Mater. 2026, 8, 1242−1257

demonstrates that the response to dCO_2 is driven by CO_2 adsorption in the MOF rather than solely by bulk pH changes.

The same experiments are repeated with a MOF-free microgel-based etalon as a reference (Figure 9(c)). The results follow a similar trend to those of the hybrid system in $NaHCO_3$, Na_2CO_3, and HCl, exhibiting red shifts under basic conditions and blue shifts under acidic conditions. This confirms that the observed swollen or deswollen states are primarily pH-dependent. In contrast to the hybrid system, the reference etalon displays a blue shift under dCO_2, similar to that observed in HCl, indicating that both responses originate from microgel deswelling driven purely by acidification rather than CO_2 adsorption. This comparison highlights that the red-shifted swelling response observed in the hybrid etalon is a direct consequence of the MOF-mediated CO_2 adsorption.

To assess the lifetime of the M&M-based etalon sensor, the response to dCO_2 is evaluated over several cycles within a time frame of 5 h. In Figure 10, $\Delta\lambda$ is computed as the difference between λ_{max} at 30 and 1 min of bubbling with CO_2. Positive $\Delta\lambda$ values demonstrate the red shift due to the swelling of the M&M hybrids as a response to dCO_2, whereas negative values indicate a blue shift associated with M&M hybrids deswelling, suggesting partial expulsion of MOF nanoparticles from the polymer matrix and a response dominated by the acidic environment generated by dCO_2. In contrast, $\Delta\lambda$ values close to zero indicate that the system has reached an equilibrium state, where no further structural changes occur, implying that the adsorption of CO_2 and polymer swelling have stabilized under the given conditions. The 5:1 BIS-cross-linked M&M-based etalon exhibits a stable response to dCO_2 for up to 3 cycles (Figure 10(a)). Cycles 1−3 show a consistent rightward peak shift ($\Delta\lambda > 0$), indicative of CO_2-induced swelling. The largest peak shift occurs in cycle 1, while cycles 2 and 3 show progressively smaller responses, suggesting partial saturation of the MOF adsorption sites. In cycle 4 $\Delta\lambda$ reaches zero, indicating an equilibrium state of the M&M hybrid system. A leftward peak shift ($\Delta\lambda < 0$) is observed in cycles 5 and 6, likely caused by microgel deswelling driven by the pH decrease associated with prolonged CO_2 bubbling. Reducing the MOF loading shortens the operational lifetime of the sensor: the 8:1 and 10:1 systems sustain measurable responses for only 2 and 1 cycles, respectively (Figure 10(b,c)).

The effect of PEGDA cross-linking on sensor lifetime is shown in Figure 10(d). The presence of PEG chains increases water content and swelling capacity of the polymeric network, leading to a lower initial $\Delta\lambda$ in cycle 1 compared to the BIS-cross-linked system. Nonetheless, the PEGDA-cross-linked sensor responds reproducibly to dCO_2 for two cycles. By cycle 3, however, negative $\Delta\lambda$ values are observed, indicating a pH-driven deswelling response of the M&M hybrids.

CONCLUSION

This work introduces hybrid microgel−MOF (M&M) hybrids as a promising pathway to design responsive sensing systems to dissolved CO_2, achieved through a novel in situ incorporation approach. The in situ incorporation of MOF (MIL-53(Al)-NH_2) during the synthesis of pNIPAm-co-MAA microgels represents an effective method for integrating MOF domains directly into the polymer network, creating structurally robust and stimuli-responsive platforms. We further unveil the decisive role of cross-linker chemistry in balancing rigidity, swelling capacity, and MOF retention within the microgel network. ICP analysis confirmed that MOF incorporation efficiency remained limited, yet despite reduced absolute adsorption compared to pristine MIL-53(Al)-NH_2, CO_2 sorption in the M&M hybrids remains significant and consistently exceeds that of microgels alone, underscoring the functional contribution of the MOF even when embedded within the polymeric matrix. UV−Vis absorbance studies further confirm that the M&M hybrids uniquely respond to CO_2 exposure through swelling-driven decreases in absorbance, highlighting the cooperative role of MOF porosity and polymer flexibility. Most importantly, the hybrid M&M-based etalons demonstrate reproducible and distinct red-shifted optical responses to dCO_2, a novelty that differentiates them from conventional microgel sensors, which respond solely to pH. This red shift originates from CO_2 adsorption into the MOF pores, which leads to a swelling-driven behavior of the M&M hybrid. Notably, this effect persists even at low MOF loadings, demonstrating that a modest amount of embedded MOF is sufficient to impart a measurable and reversible optical response. Cyclic reflectance measurements confirm the reversibility and stability of the optical response over multiple CO_2 adsorption cycles, underscoring the robustness of the hybrid design. By directly coupling MOF-mediated CO_2 adsorption with optical output, M&M-based etalons represent a new generation of tunable, in situ sensing platforms with significant potential for deployment in environmental monitoring, carbon capture, and negative emission technologies. Given that ocean acidification is fundamentally driven by rising dCO_2 levels, the CO_2-specific swelling mechanism demonstrated here suggests that the platform could, in principle, be adapted for monitoring such environmental changes. Although sensitivity under complex ionic conditions and evaluation under realistic seawater conditions remain areas of future work, establishing this CO_2-selective response provides a valuable foundation for extending the technology toward broader aquatic sensing applications. Improved anchoring strategies and/or alternative synthesis routes need to be further investigated to overcome limited MOF retention within the microgel network, enhancing long-term stability. Thermal conditions can modulate pNIPAm swelling behavior; hence, future studies should also assess the effect of temperature on CO_2 responsiveness, complementing efforts to improve MOF loading, microgel cross-linking density, and hybrid chemical stability. Overall, the results presented here firmly establish the M&M-based etalon as a breakthrough concept in dCO_2 detection, opening new avenues for responsive, multifunctional sensing technologies.

ASSOCIATED CONTENT

Supporting Information

The Supporting Information is available free of charge at https://pubs.acs.org/doi/10.1021/acsapm.5c04112.

Characterization results for MIL-53(Al)-NH_2, pNIPAm-co-MAA microgels, and the M&M hybrids are included in the Supporting Information; particularly, thermogravimetric analysis (TGA); powder X-ray diffraction (PXRD); and scanning electron microscopy (SEM); particle size; ζ-potential; UV−Vis absorbance; and CO_2 adsorption; the class will automatically add a sentence pointing to the information online (PDF)

https://doi.org/10.1021/acsapm.5c04112
ACS Appl. Polym. Mater. 2026, 8, 1242−1257

AUTHOR INFORMATION

Corresponding Author

Hanieh Bazyar − *Transport Phenomena, Chemical Engineering Department, Faculty of Applied Sciences, Delft University of Technology, 2629HZ Delft, The Netherlands;* orcid.org/0000-0003-1689-9826; Phone: +31(0) 152782760; Email: h.bazyar@tudelft.nl

Authors

Georgia Kontaxi − *Transport Phenomena, Chemical Engineering Department, Faculty of Applied Sciences, Delft University of Technology, 2629HZ Delft, The Netherlands*

Klaartje Roovers − *Transport Phenomena, Chemical Engineering Department, Faculty of Applied Sciences, Delft University of Technology, 2629HZ Delft, The Netherlands*

Michael J. Serpe − *Department of Chemistry, University of Alberta, T6G 2G2 Edmonton, Canada*

Complete contact information is available at: https://pubs.acs.org/10.1021/acsapm.5c04112

Notes

The authors declare no competing financial interest.

ACKNOWLEDGMENTS

H. Bazyar would like to thank the Climate Action Program at the TU Delft for funding this project. The authors acknowledge Professor J. Stryker from the University of Alberta and Dr. M.A.van der Veen from the Delft University of Technology, for their insight on MOF synthesis and the use of lab facilities. The authors further thank C. Huang, a PhD candidate at the Faculty of Applied Sciences, Delft University of Technology, for helping during the synthesis procedure of MOF.

REFERENCES

(1) Feely, R. A.; Doney, S. C.; Cooley, S. R. Ocean acidification: Present conditions and future changes in a high-CO world. *Oceanography* **2009**, *22*, 36−47.

(2) Caldeira, K.; Wickett, M. E. Anthropogenic carbon and ocean pH. *Nature* **2003**, *425*, 365.

(3) Gattuso, J. P.; Frankignoulle, M.; Bourge, I.; Romaine, S.; Buddemeier, R. W. Effect of calcium carbonate saturation of seawater on coral calcification. *Global Planet. Change* **1998**, *18*, 37−46.

(4) Branch, T. A.; DeJoseph, B. M.; Ray, L. J.; Wagner, C. A. Impacts of ocean acidification on marine seafood. *Trends Ecol. Evol.* **2013**, *28*, 178−186.

(5) Pires, J. Negative emissions technologies: A complementary solution for climate change mitigation. *Sci. Total Environ.* **2019**, *672*, 502−514.

(6) de Lannoy, C.-F.; Eisaman, M. D.; Jose, A.; Karnitz, S. D.; DeVaul, R. W.; Hannun, K.; Rivest, J. L. B. Indirect ocean capture of atmospheric CO2: Part I. Prototype of a negative emissions technology. *Int. J. Greenhouse Gas Control* **2018**, *70*, 243−253.

(7) Karunarathne, S.; Andrenacci, S.; Carranza-Abaid, A.; Jayarathna, C.; Maelum, M.; Skagestad, R.; Aksel Haugen, H. Review on CO2 removal from ocean with an emphasis on direct ocean capture (DOC) technologies. *Sep. Purif. Technol.* **2025**, *353*, No. 128598.

(8) Impacts of Ocean Acidification on Coral Reefs and Other Marine Calcifiers. https://www.usgs.gov/centers/spcmsc/news/co2-calc-user-friendly-seawater-carbon-calculator-windows-mac-os-x-and-ios 2011 (accessed September 2025).

(9) De Lannoy, C.-F.; Eisaman, M. D.; Jose, A.; Karnitz, S. D.; DeVaul, R. W.; Hannun, K.; Rivest, J. L. Indirect ocean capture of atmospheric CO2: Part I. Prototype of a negative emissions technology. *Int. J. Greenhouse Gas Control* **2018**, *70*, 243−253.

(10) Prien, R. D. The future of chemical in situ sensors. *Marine Chem.* **2007**, *107*, 422−432.

(11) Gao, Y.; Li, X.; Serpe, M. J. Stimuli-responsive microgel-based etalons for optical sensing. *Rsc Adv.* **2015**, *5*, 44074−44087.

(12) Wang, J.; Zhang, X.; Shi, K.; Zhang, Q. Optical Devices Constructed From Responsive Microgels for Polyphenols Detection. *Front. Chem.* **2021**, *9*, No. 580025.

(13) Nam, S.; Kim, H.; Lee, S.-M.; Durukan, M. B.; Unalan, H. E.; Lee, H. J. A glucose-responsive microgel-based soft etalon as an epidermal glucose colorimetric sensor. *Sens. Actuators, B* **2023**, *396*, No. 134554.

(14) Kontaxi, G.; Lugtmeijer, T.; Serpe, M.; Bazyar, H. Inkjet-printed microgel-based etalon sensor. *Biomicrofluidics* **2025**, *19*, No. 044101, DOI: 10.1063/5.0252901.

(15) Islam, M. R.; Serpe, M. J. Label-free detection of low protein concentration in solution using a novel colorimetric assay. *Biosens. Bioelectron.* **2013**, *49*, 133−138.

(16) Kontaxi, G.; Wensink, G.; Sberna, P.; Rücker, M.; Garbin, V.; Serpe, M.; Bazyar, H. Microgel-based etalon membranes: Characterization and properties. *APL Mater.* **2024**, *12*, No. 091113.

(17) Zhang, M.; Loeve, A. J.; Serpe, M. J.; Bazyar, H. Etalon@ lateral flow strip for integrated separation-sensing microfluidic platforms. *Biosens. Bioelectron.* **2025**, *287*, No. 6.

(18) Sorrell, C. D.; Carter, M. C. D.; Serpe, M. J. A "Paint-On" Protocol for the Facile Assembly of Uniform Microgel Coatings for Color Tunable Etalon Fabrication. *ACS Appl. Mater. Interfaces* **2011**, *3*, 1140−1147.

(19) Zhang, Q. M.; Xu, W.; Serpe, M. J. Optical Devices Constructed from Multiresponsive Microgels. *Angew. Chem., Int. Ed.* **2014**, *53*, 4827−4831.

(20) Sorrell, C. D.; Carter, M. C. D.; Serpe, M. J. Color Tunable Poly (N-Isopropylacrylamide)-co-Acrylic Acid Microgel-Au Hybrid Assemblies. *Adv. Funct. Mater.* **2011**, *21*, 425−433.

(21) Zhang, Q. M.; Ahiabu, A.; Gao, Y.; Serpe, M. J. CO_2-switchable poly (N-isopropylacrylamide) microgel-based etalons. *J. Mater. Chem. C* **2015**, *3*, 495−498.

(22) Kim, S.; Lee, K.; Cha, C. Refined control of thermoresponsive swelling/deswelling and drug release properties of poly (N-isopropylacrylamide) hydrogels using hydrophilic polymer cross-linkers. *J. Biomater. Sci., Polym. Ed.* **2016**, *27*, 1698−1711.

(23) Wellert, S.; Richter, M.; Hellweg, T.; von Klitzing, R.; Hertle, Y. Responsive Microgels at Surfaces and Interfaces. *Z. Phys. Chem.* **2015**, *229*, 1225−1250.

(24) Yu, D.; Xiao, X.; Shokoohi, C.; Wang, Y.; Sun, L.; Juan, Z.; Kipper, M. J.; Tang, J.; Huang, L.; Han, G. S.; Jung, H. S.; Chen, J. Recent Advances in Stimuli-Responsive Smart Membranes for Nanofiltration. *Adv. Funct. Mater.* **2023**, *33*, No. 2211983.

(25) Gupta, D. K.; Karthickeyan, D.; Tata, B. V. R.; Ravindran, T. R. Temperature-driven volume phase transition of a single stimuli-responsive microgel particle using optical tweezers. *Colloid Polym. Sci.* **2016**, *294*, 1901−1908.

(26) Lue, S. J.; Chen, B.-W.; Shih, C.-M.; Chou, F.-Y.; Lai, J.-Y.; Chiu, W.-Y. Micron- and Nano-sized Poly(N-isopropylacrylamide-co-acrylic acid) Latex Syntheses and Their Applications for Controlled Drug Release. *J. Nanosci. Nanotechnol.* **2013**, *13*, 5305−5315.

(27) Norouzi Farahani, E.; Arzemanzadeh, S.; Mahnama, M.; Hosseinian, E. Atomistic insights into the mechanical properties of cross-linked Poly(N-isopropylacrylamide) hydrogel. *Polymer* **2024**, *297*, No. 126798.

(28) Sorrell, C. D.; Serpe, M. J. Reflection Order Selectivity of Color-Tunable Poly(N-isopropylacrylamide) Microgel Based Etalons. *Adv. Mater.* **2011**, *23*, 4088−4092.

(29) Begum, R.; Farooqi, Z. H.; Ahmed, E.; Sharif, A.; Wu, W.; Irfan, A. Fundamentals and applications of acrylamide based microgels and their hybrids: a review. *RSC Adv.* **2019**, *9*, 13838−13854.

(30) Ma, X.; Cui, Y.; Zhao, X.; Zheng, S.; Tang, X. Different deswelling behavior of temperature-sensitive microgels of poly(N-

isopropylacrylamide) crosslinked by polyethyleneglycol dimethacrylates. *J. Colloid Interface Sci.* **2004**, *276*, 53−59.
(31) Pelton, R. Temperature-sensitive aqueous microgels. *Adv. Colloid Interface Sci.* **2000**, *85*, 1−33.
(32) Agnihotri, P.; Aery, S. S.; Dan, A. Temperature- and pH-responsive poly(N-isopropylacrylamide-co-methacrylic acid) microgels as a carrier for controlled protein adsorption and release. *Soft Matter* **2021**, *17*, 9595−9606.
(33) Guan, X.; Liu, Y.; Li, L.; Kwok, M.-H.; Ding, M.; Jiang, H.; Ngai, T. Dynamic Assembly of Microgels and Polymers at Non-Aqueous Liquid/Liquid Interfaces. *Adv. Sci.* **2025**, *12*, No. 2415642.
(34) Liu, T.; Seiffert, S.; Thiele, J.; Abate, A. R.; Weitz, D. A.; Richtering, W. Non-coalescence of oppositely charged droplets in pH-sensitive emulsions. *Proc. Natl. Acad. Sci. U.S.A.* **2012**, *109*, 384−389.
(35) Carvalho, W. S.; Lee, C.; Zhang, Y.; Czarnecki, A.; Serpe, M. J. Probing the response of poly (N-isopropylacrylamide) microgels to solutions of various salts using etalons. *J. Colloid Interface Sci.* **2021**, *585*, 195−204.
(36) Li, J.-R.; Kuppler, R. J.; Zhou, H.-C. Selective gas adsorption and separation in metal-organic frameworks. *Chem. Soc. Rev.* **2009**, *38*, 1477−1504.
(37) Li, D.; Yadav, A.; Zhou, H.; Roy, K.; Thanasekaran, P.; Lee, C. Advances and applications of metal-organic frameworks (MOFs) in emerging technologies: a comprehensive review. *Global Chall.* **2024**, *8*, No. 2300244.
(38) Allegretto, J. A.; Giussi, J. M.; Moya, S. E.; Azzaroni, O.; Rafti, M. Synthesis and characterization of thermoresponsive ZIF-8@PNIPAm-co-MAA microgel composites with enhanced performance as an adsorption/release platform. *RSC Adv.* **2020**, *10*, 2453−2461.
(39) Zhang, F.; Zou, X.; Gao, X.; Fan, S.; Sun, F.; Ren, H.; Zhu, G. Hydrogen Selective NH_2 -MIL-53(Al) MOF Membranes with High Permeability. *Adv. Funct. Mater.* **2012**, *22*, 3583−3590.
(40) Serra-Crespo, P.; van der Veen, M. A.; Gobechiya, E.; Houthoofd, K.; Filinchuk, Y.; Kirschhock, C. E. A.; Martens, J. A.; Sels, B. F.; De Vos, D. E.; Kapteijn, F.; Gascon, J. NH2-MIL-53(Al): A High-Contrast Reversible Solid-State Nonlinear Optical Switch. *J. Am. Chem. Soc.* **2012**, *134*, 8314−8317.
(41) Toh, J. E.; Lee, C. S.; Lim, W. H.; Pichika, M. R.; Chua, B. W. Stimulus-responsive MOF—hydrogel composites: Classification, preparation, characterization, and their advancement in medical treatments. *Open Chem.* **2024**, *22*, No. 20240061.
(42) Noorani, N.; Mehrdad, A. Impregnation of amine functionalized deep eutectic solvents in NH2-MIL-53 (Al) MOF for CO2/N2 separation. *Sci. Rep.* **2023**, *13*, No. 13012.
(43) Zimpel, A.; Preiß, T.; Röder, R.; Engelke, H.; Ingrisch, M.; Peller, M.; Rädler, J. O.; Wagner, E.; Bein, T.; Lächelt, U.; Wuttke, S. Imparting Functionality to MOF Nanoparticles by External Surface Selective Covalent Attachment of Polymers. *Chem. Mater.* **2016**, *28*, 3318−3326.
(44) Maan, O.; Song, P.; Chen, N.; Lu, Q. An In Situ Procedure for the Preparation of Zeolitic Imidazolate Framework-8 Polyacrylamide Hydrogel for Adsorption of Aqueous Pollutants. *Adv. Mater. Interfaces* **2019**, *6*, No. 1801895.
(45) Sun, W.; Zhao, X.; Webb, E.; Xu, G.; Zhang, W.; Wang, Y. Advances in metal-organic framework-based hydrogel materials: preparation, properties and applications. *J. Mater. Chem. A* **2023**, *11*, 2092−2127.
(46) McDonald, K. A.; Feldblyum, J. I.; Koh, K.; Wong-Foy, A. G.; Matzger, A. J. Polymer@MOF@MOF: "grafting from" atom transfer radical polymerization for the synthesis of hybrid porous solids. *Chem. Commun.* **2015**, *51*, 11994−11996.
(47) Gamage, N. H.; McDonald, K. A.; Matzger, A. J. MOF-5-Polystyrene: direct production from monomer, improved hydrolytic stability, and unique guest adsorption. *Angew. Chem., Int. Ed.* **2016**, *55*, 12099−12103.
(48) Nagata, S.; Kokado, K.; Sada, K. Metal-organic framework tethering PNIPAM for ON-OFF controlled release in solution. *Chem. Commun.* **2015**, *51*, 8614−8617.
(49) Yao, B.-J.; Fu, Q.-J.; Li, A.-X.; Zhang, X.-M.; Li, Y.-A.; Dong, Y.-B. A thermo-responsive polymer-tethered and Pd NP loaded UiO-66 NMOF for biphasic CB dechlorination. *Green Chem.* **2019**, *21*, 1625−1634.
(50) Chen, X.; Zhuang, Y.; Rampal, N.; Hewitt, R.; Divitini, G.; O'Keefe, C. A.; Liu, X.; Whitaker, D. J.; Wills, J. W.; Jugdaohsingh, R.; et al. Formulation of metal-organic framework-based drug carriers by controlled coordination of methoxy PEG phosphate: boosting colloidal stability and redispersibility. *J. Am. Chem. Soc.* **2021**, *143*, 13557−13572.
(51) Huang, C.; Najafabadi, S. A. N.; Albertsma, J.; Rook, W.; Fischer, M.; Hartmann, M.; van der Veen, M. A. Capturing CO2 under Dry and Humid Conditions: When Does the Parent MOF Outperform the MTV MOF? *Inorg. Chem.* **2025**, *64*, 18916−18924.
(52) Dickson, A. G.; Sabine, C. L.; Christian, J. R. *Guide to Best Practices for Ocean CO2 Measurements*; North Pacific Marine Science Organization, 2007.
(53) Haghi, R. K.; Chapoy, A.; Peirera, L. M.; Yang, J.; Tohidi, B. pH of CO2 saturated water and CO2 saturated brines: Experimental measurements and modelling. *Int. J. Greenhouse Gas Control* **2017**, *66*, 190−203.
(54) Loiseau, T.; Serre, C.; Huguenard, C.; Fink, G.; Taulelle, F.; Henry, M.; Bataille, T.; Férey, G. A rationale for the large breathing of the porous aluminum terephthalate (MIL-53) upon hydration. *Chem. - Eur. J.* **2004**, *10*, 1373−1382.
(55) Ge, J.; Liu, L.; Qiu, L.; Jiang, X.; Shen, Y. Facile synthesis of amine-functionalized MIL-53 (Al) by ultrasound microwave method and application for CO2 capture. *J. Porous Mater.* **2016**, *23*, 857−865.
(56) Vialetto, J.; Ramakrishna, S. N.; Stock, S.; Von Klitzing, R.; Isa, L. Modulating the conformation of microgels by complexation with inorganic nanoparticles. *J. Colloid Interface Sci.* **2024**, *672*, 797−804.
(57) Backes, S.; Von Klitzing, R. Nanomechanics and nanorheology of microgels at interfaces. *Polymers* **2018**, *10*, No. 978.
(58) Hu, S.; Fang, Y.; Liang, C.; Turunen, M.; Ikkala, O.; Zhang, H. Thermally trainable dual network hydrogels. *Nat. Commun.* **2023**, *14*, No. 3717.
(59) Wang, R.; Cheng, C.; Wang, H.; Wang, D. Swollen hydrogel nanotechnology: Advanced applications of the rudimentary swelling properties of hydrogels. *ChemPhysMater* **2024**, *3*, 357−375.
(60) Chen, X. Y.; Hoang, V.-T.; Rodrigue, D.; Kaliaguine, S. Optimization of continuous phase in amino-functionalized metal-organic framework (MIL-53) based co-polyimide mixed matrix membranes for CO 2/CH 4 separation. *RSC Adv.* **2013**, *3*, 24266−24279.
(61) Mileo, P. G. M.; Yuan, S.; Ayala, S., Jr.; Duan, P.; Semino, R.; Cohen, S. M.; Schmidt-Rohr, K.; Maurin, G. Structure of the polymer backbones in polyMOF materials. *J. Am. Chem. Soc.* **2020**, *142*, 10863−10868.
(62) Kalaj, M.; Cohen, S. M. Postsynthetic modification: an enabling technology for the advancement of metal-organic frameworks. *ACS Cent. Sci.* **2020**, *6*, 1046−1057.
(63) Jeong, H.-S.; Kim, E.; Park, J. P.; Lee, S.-J.; Lee, H.; Choi, C.-H. Broad-temperature-range mechanically tunable hydrogel microcapsules for controlled active release. *J. Controlled Release* **2023**, *356*, 337−346.
(64) Wilms, D.; Adler, Y.; Schröer, F.; Bunnemann, L.; Schmidt, S. Elastic modulus distribution in poly(N -isopopylacrylamide) and oligo(ethylene glycol methacrylate)-based microgels studied by AFM. *Soft Matter* **2021**, *17*, 5711−5717.
(65) Birdi, K. S. *Handbook of Surface and Colloid Chemistry*; CRC Press, 2008.
(66) Mayerhöfer, T. G.; Pahlow, S.; Popp, J. The Bouguer-Beer-Lambert law: Shining light on the obscure. *ChemPhysChem* **2020**, *21*, 2029−2046.
(67) Ponomareva, E.; Tadgell, B.; Hildebrandt, M.; Krüsmann, M.; Prévost, S.; Mulvaney, P.; Karg, M. The fuzzy sphere morphology is responsible for the increase in light scattering during the shrinkage of thermoresponsive microgels. *Soft Matter* **2022**, *18*, 807−825.

https://doi.org/10.1021/acsapm.5c04112
ACS Appl. Polym. Mater. 2026, 8, 1242−1257

(68) Zygadlo, K.; Liu, C.-H.; Bernardo, E. R.; Ai, H.; Nieh, M.-P.; Hanson, L. A. Correlating structural changes in thermoresponsive hydrogels to the optical response of embedded plasmonic nanoparticles. *Nano Adv.* **2023**, *6*, 146−154.
(69) Han, F.; Soeriyadi, A. H.; Vivekchand, S. R. C.; Gooding, J. J. Simple Method for Tuning the Optical Properties of Thermoresponsive Plasmonic Nanogels. *ACS Macro Lett.* **2016**, *5*, 626−630.
(70) Tran, T. V.; Jalil, A. A.; Nguyen, D. T. C.; Alhassan, M.; Nabgan, W.; Cao, A. N. T.; Nguyen, T. M.; Vo, D.-V. N. A critical review on the synthesis of NH2-MIL-53 (Al) based materials for detection and removal of hazardous pollutants. *Environ. Res.* **2023**, *216*, No. 114422.
(71) Sj, G.; Sing, K. *Adsorption, Surface Area and Porosity*. Acad Press, NY, 1982.
(72) Thommes, M.; Kaneko, K.; Neimark, A. V.; Olivier, J. P.; Rodriguez-Reinoso, F.; Rouquerol, J.; Sing, K. S. Physisorption of gases, with special reference to the evaluation of surface area and pore size distribution (IUPAC Technical Report). *Pure Appl. Chem.* **2015**, *87*, 1051−1069.
(73) Rouquerol, J.; Rouquerol, F.; Llewellyn, P.; Maurin, G.; Sing, K. *Adsorption by Powders and Porous Solids: Principles, Methodology and Applications*; Academic Press, 2013.
(74) Redwine, G. E. B.; Braunecker, W. A.; Gennett, T. Polymer Encapsulated Framework Materials for Enhanced Gas Storage and Separations. *ACS Mater. Au* **2025**, *5*, 268−298.
(75) Liu, J.; Li, B.; Martins, V.; Huang, Y.; Song, Y. Enhancing CO2 Adsorption in MIL-53(Al) through Pressure-Temperature Modulation: Insights from Guest-Host Interactions. *J. Phys. Chem. C* **2024**, *128*, 8007−8015.
(76) Sabetghadam, A.; Seoane, B.; Keskin, D.; Duim, N.; Rodenas, T.; Shahid, S.; Sorribas, S.; Guillouzer, C. L.; Clet, G.; Tellez, C.; et al. Metal organic framework crystals in mixed-matrix membranes: impact of the filler morphology on the gas separation performance. *Adv. Funct. Mater.* **2016**, *26*, 3154−3163.
(77) Horcajada, P.; Gref, R.; Baati, T.; Allan, P. K.; Maurin, G.; Couvreur, P.; Férey, G.; Morris, R. E.; Serre, C. Metal-organic frameworks in biomedicine. *Chem. Rev.* **2012**, *112*, 1232−1268.
(78) Kalaj, M.; Bentz, K. C.; Ayala, S. J.; Palomba, J. M.; Barcus, K. S.; Katayama, Y.; Cohen, S. M. MOF-Polymer Hybrid Materials: From Simple Composites to Tailored Architectures. *Chem. Rev.* **2020**, *120*, 8267−8302.
(79) Pander, M.; Gil-San-Millan, R.; Delgado, P.; Perona-Bermejo, C.; Kostrzewa, U.; Kaczkowski, K.; Kubicki, D. J.; Navarro, J. A.; Bury, W. MOF/polymer hybrids through in situ free radical polymerization in metal-organic frameworks. *Mater. Horiz.* **2023**, *10*, 1301−1308.

https://doi.org/10.1021/acsapm.5c04112
ACS Appl. Polym. Mater. 2026, 8, 1242−1257